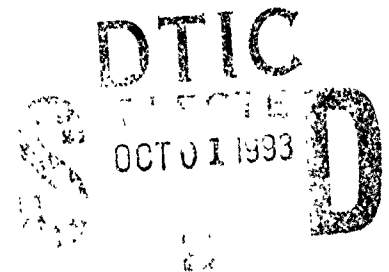AD-A270 001

RL-TR-92-159
In-House Report
June 1992

# STATISTICAL DESCRIPTION OF THE BISTATIC RADAR CROSS SECTION DISTRIBUTIONS FOR A RIGHT CIRCULAR CYLINDER

Richard L. Wittschen, 1Lt, USAF

DTIC

OCT 0 1 1993

93-22836

This report has been reviewed by the Rome Laboratory Public Affairs Office (PA) and is releasable to the National Technical Information Service (NTIS). At NTIS it will be releasable to the general public, including foreign nations.

RL-TR-92-159 has been reviewed and is approved for publication.

APPROVED: *[signature]*

EDWARD E. ALTSHULER
Chief, Applied Electromagnetics Division
Electromagnetics & Reliability Directorate

FOR THE COMMANDER: *[signature]*

JOHN K. SCHINDLER, Director
Electromagnetics & Reliability Directorate

# REPORT DOCUMENTATION PAGE

Public reporting burden for this collection of information is estimated to average 1 hour per response, including the time for reviewing instructions, searching existing data sources, gathering and maintaining the data needed, and completing and reviewing the collection of information. Send comments regarding this burden estimate or any other aspect of this collection of information, including suggestions for reducing this burden to Washington Headquarters Services Directorate for Information Operations and Reports, 1215 Jefferson Davis Highway, Suite 1204, Arlington, VA 22202-4302, and to the Office of Management and Budget Paperwork Reduction Project (0704-0188), Washington, DC 20503.

| 1. AGENCY USE ONLY (Leave blank) | 2. REPORT DATE June 1992 | 3. REPORT TYPE AND DATES COVERED In-House January 91 to April 92 |
|---|---|---|

**4. TITLE AND SUBTITLE**
Statistical Description of the Bistatic Radar Cross Section Distributions for a Right Circular Cylinder

**5. FUNDING NUMBERS**
PE 62702F
PR 4600
TA 15
WU 06

**6. AUTHOR(S)**

Richard L. Wittschen, 1LT, USAF

**7. PERFORMING ORGANIZATION NAME(S) AND ADDRESS(ES)**

Rome Laboratory (ERCT)
31 Grenier Street
Hanscom AFB, MA 01731-3010

**8. PERFORMING ORGANIZATION REPORT NUMBER**

RL-TR-92-159

**9. SPONSORING/MONITORING AGENCY NAME(S) AND ADDRESS(ES)**

**10. SPONSORING/MONITORING AGENCY REPORT NUMBER**

**11. SUPPLEMENTARY NOTES**

**12a. DISTRIBUTION/AVAILABILITY STATEMENT**

Approved for public release; distribution unlimited

**12b. DISTRIBUTION CODE**

**13. ABSTRACT (Maximum 200 words)**

Detection probabilities for monostatic and bistatic radars are compared by computer simulation. The computer generated radar cross section (RCS) of a long thin cylinder is utilized in the computation of detection probabilities for both the monostatic and bistatic configurations. The statistics of the RCS distributions are used to determine the best characterizing function for the cylinder data. It is shown that the beta distribution provides the most accurate description of the cylinder RCS for both configurations. The beta distribution is used as the fluctuation model for the RCS of the cylinder, and in the determination of the probability of detection. Comparison of detection probabilities shows that the detection probabilities for large angle bistatic cases are greater than for the monostatic case.

**14. SUBJECT TERMS**
Bistatic
Radar cross section
Bistatic radar

**15. NUMBER OF PAGES**
56

**16. PRICE CODE**

| 17 SECURITY CLASSIFICATION OF REPORT | 18. SECURITY CLASSIFICATION OF THIS PAGE | 19 SECURITY CLASSIFICATION OF ABSTRACT | 20. LIMITATION OF ABSTRACT |
|---|---|---|---|

# Acknowledgements

I express my appreciation to Dr. Leon Poirier, his assistance in completing this project was invaluable. Others who contributed toward the completion of this work are; Jim Schmitz, Dr. Keith Trott, Dr. Robert McGahan, and Francis Shin. I thank them all for their assistance.

| Accesion For | |
|---|---|
| NTIS CRA&I | ☒ |
| DTIC TAB | ☐ |
| Unannounced | ☐ |
| Justification | |
| By | |
| Dist. ibution / | |
| Availability Codes | |
| Dist | Avail and / or Special |
| A-1 | |

DTIC QUALITY INSPECTED 1

# Contents

## Tables

# Statistical Description of the Bistatic Radar Cross-Section Distributions for a Right Circular Cylinder

## 1  INTRODUCTION

Most radar systems in use are monostatic, that is, a common antenna is used for transmitting and receiving. A bistatic radar uses two antennas that are separated (or two collocated antennas) separated enough so that the (bistatic) angle between the lines-of-sight from each antenna to the target is significant. The early radar experiments were bistatic.[1] With the development of the duplexer, it was possible to use one antenna for both transmitting and receiving (monostatic radar). The duplexer allows the receiver circuits to be isolated from the antenna during transmission and the transmitting circuits to be isolated during reception. Without this isolation, the receiving circuits are susceptible to damage from the transmitting circuits during transmission, and the transmitting circuits may introduce noise into the receiving circuits during reception of incoming signals. From this point on, monostatic radar became the most prevalent system and the interest in bistatic radar declined.

The separation of transmitter and receiver in a bistatic radar increases the difficulty of deploying the system. Now target detections can occur only within the overlap region of the two beams. The location of this region depends on the beam pointing directions and the time elapsed from the transmission of the radar signal. It is apparent that control of the surveillance area range-angle resolution cells requires precise knowledge of the location of the antennas, their pointing directions, and the timing of the radar waveform. Coherent signal processing further requires phase synchronization between transmitter and receiver.

In the past it was believed that any benefits that might arise from bistatic radar were not worth overcoming the complexities associated with such a system[2] but technological

[1] Skolnik, M.I. (1970) *Radar Handbook*, McGraw-Hill Inc., New York.
[2] Skolnik, M.I. (1961) An Analysis of Bistatic Radar, *IRE Trans. Aero. and Nav. Electron.*, 8:19-27

advances have made the deployment of a bistatic system more feasible, and in recent years, there has been renewed interest in bistatic radar. Several bistatic radar systems have been proposed and some systems are in use today.[3]

Our interest in bistatic radar stems from two phenomena that for some targets occur at large bistatic angles; radar cross section enhancement and reduced radar cross section fluctuation rates.[4] Reduced radar cross section (RCS) amplitude fluctuations refers to the changes in the magnitude and its rate of change with bistatic angle. RCS enhancement refers to the increase of the average level of RCS with increasing bistatic angle $\beta$. These characteristics may provide a bistatic radar with improved performance over a monostatic radar for some applications. It is this improved performance that is investigated in this report. Emphasis is on the fluctuation reduction with increasing bistatic angle and the performance improvement is quantified by the comparison of detection probabilities for both monostatic and bistatic cases.

The problem is to determine whether or not a bistatic configuration provides improved detection probabilities compared to the monostatic configuration. A statistical distribution is fitted to the computer generated target RCS for both the monostatic and bistatic cases and the detection probabilities compared. In this analysis, computer generated radar cross section (RCS) of a long thin cylinder is used, for both the monostatic and bistatic configurations. These effects dominate for large bistatic angles, that is for bistatic angles in the range 100 to 170°.

It has been shown that the beta distribution provides an accurate description for the RCS of complex bodies[5], including the cylinder for the bistatic and monostatic cases. The beta distribution is used as the fluctuation model for this object in both monostatic and bistatic cases. The evaluation of the detection probabilities follows Marcum and Swerling's work on detection probabilities.[6,7] The comparison of detection probabilities for both the monostatic and bistatic configurations is then used as a measure of the performance of each system.

## 2   THEORY OF BISTATIC RADAR CROSS SECTION

This chapter addresses the differences in electromagnetic scattering between the monostatic and bistatic configurations, and relates how these differences account for the RCS enhancement and the reduced amplitude fluctuation rate. The received signal in the bistatic case differs from the received signal in the monostatic case. The majority of the received signal in the monostatic case is the backscatter, the energy scattered directly back to the radar site, from the object of interest. The received signal in the bistatic case, depending upon the bistatic angle, can be similar to the backscatter or forward scatter; that is, the energy scattered from the object in the opposite direction of the transmitter. The statistics of RCS fluctuations also vary from the monostatic to the bistatic case. The

[3] Mitchell, B. (1988) European Firms Target Development of Bistatic Radar, *Microwaves & RF*, 27(3):49-54.

[4] Paddison, F.C., Follin, J.W., and Mitchell, F. (1985) Large Bistatic Angle Radar Cross Section of a Right Circular Cylinder,*Electromagnetics*, 5:63-77.

[5] Follin, J.W., Paddison, F.C., and Maffett, A.L. (1984) Statistics of Radar Cross Section Scintillations, *Journal of Electromagnetics*, 4:139-164.

[6] Marcum, J.I. (1960) A Statistical Theory of Target Detection by a Pulsed Radar, *IRE Trans. Inform. Theory.*, IT-6: 145-267

[7] Swerling, P. (1960) Probability of Detection for Fluctuating Targets, *IRE Trans. Inform. Theory*, IT-6:65-217.

RCS amplitude fluctuation rate is reduced in the bistatic case, that is, the amplitude fluctuation rate decreases as the bistatic angle is increased.

## 2.1 Forward Scattering

Before the discussion of forward scattering, it is helpful to introduce the basic principles of electromagnetic scattering. When an electromagnetic wave is incident upon an object, reflection, refraction, absorption, and diffraction of energy occurs. Electromagnetic scattering encompasses all of these. The scattered field is introduced to aid in this analysis. The scattered field ($E_{SCAT}$) and the incident field ($E_{INC}$), through superposition, represent the total field ($E_{TOT}$). That is, $E_{TOT} = E_{SCAT} + E_{INC}$ .

Figure 1 shows an incident plane wave on a sphere. Electromagnetic energy is scattered in all directions. The energy returned back to the source is referred to as the backscatter, and the energy that continues away from the source and target is the forward scatter. In general, in the forward region, the scattered field will be larger than the backscatter from the target. This can be understood by looking at the scattered field,

$$E_{SCAT} = E_{TOT} - E_{INC}. \tag{1}$$

The incident field induces electric currents on the target. These currents distribute themselves such that a radiation pattern is produced in all directions. The incident field that would be present within the shadow region if the target were absent is cancelled by the scattered field reradiated by the currents induced in the target. Therefore $E_{INC}$ is very small and the scattered field in this direction is equivalent to the incident field over the physical cross section of the target with opposite phase. Thus, we see a large forward scattered lobe with a peak RCS given by

$$\sigma_f = 4\pi A^2/\lambda^2, \tag{2}$$

where A is the area of the shadow; the total projected area of the object as viewed by the transmitter.[8] Note that this RCS is determined by the physical area of the target and the wavelength of the incident wave.

The lobe pattern is the antenna pattern of a uniformly illuminated flat antenna in the shape of the shadow. Thus, for a rectangular shadow, the lobe pattern will be that of a rectangular flat antenna; ($\frac{\sin x}{x}$). The peak RCS of the forward scatter lobe will be along the path of the original transmission; $\beta = 180°$. The lobe pattern allows a receiver off the line of the original transmission to receive a significant portion of the forward scattered signal. That is, a system with a bistatic angle of 150° lies within the forward scatter lobe, so that the amplitude of the RCS is greater than the monostatic RCS amplitude.

Scattering from spheres has received much attention in the literature and the exact solutions for the scattered fields have been determined by Mie.[9] These solutions have been incorporated into a computer program to determine the scattering from a sphere at different bistatic angles.[10] Figures 2 and 3 show the E-plane and H-plane scattering from

[8] Barton, D.K. (1988) *Modern Radar System Analysis*, Artech House, Norwood, MA.

[9] Mie, G. (1908) *Ann. d. Physik*, 25:377-442.

[10] DiBeneditto, J.P. (1984) *Bistatic Scattering From Conducting Calibration Spheres*, RADC-TR-84-93, Hanscom AFB, MA.
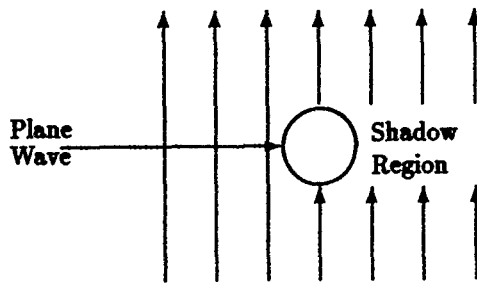
Figure 1. Shadow Region

a sphere versus the bistatic angle, and shows the lobe structure of the forward scatter. From these figures, the RCS enhancement is more pronounced at bistatic angles ranging from $150 - 180°$. Thus, a bistatic radar system configured with a bistatic angle of $150°$ receives a signal greater than the received signal from a monostatic configuration.

## 2.2 Reduced RCS Fluctuations

The relative path lengths to and from the many scattering centers that make up a target vary as the target's aspect angle changes. This causes the relative phases of the individual scattering fields to vary as well. Thus the component signals sometimes interfere constructively and sometimes destructively. It is this phenomenon that causes the RCS to be such a sensitive function of aspect. It is not unusual to observe changes of 20-30 dB in the RCS of an aircraft target for aspect angle changes of much less than one degree. Because of uncertainties in aspect angle and detailed target geometry, it is not possible to describe the fine structure of these variations and instead they are called RCS fluctuations and described in statistical terms.

The amplitude and width (measured in aspect angle) of these fluctuations decreases steadily as the bistatic angle increases. In fact, for $\beta = 180°$ the fluctuations can disappear completely; the RCS is independent of aspect and depends (for targets large compared to the wavelength) only on the projected area of the target as discussed in connection with Equation (2). To demonstrate the dependence of the RCS on aspect angle and to show the effects of increasing the bistatic angle, we will calculate the monostatic and bistatic RCS of a simple barbell made up of two conducting spheres attached to the ends of a rigid rod. The analysis assumes that the cross section of the rod is zero, the bistatic cross section of the sphere is independent of bistatic angle, the spheres do not shadow one another, no multiple scattering between the spheres occurs, and the dumbbell is in the field of the radar antenna.

In Figure 4, the magnitudes and phases of scattered electric fields $E_1$ and $E_2$ at the receiving antenna depend on the RCS of the spheres ($\sigma_1$ and $\sigma_2$) and the total path lengths
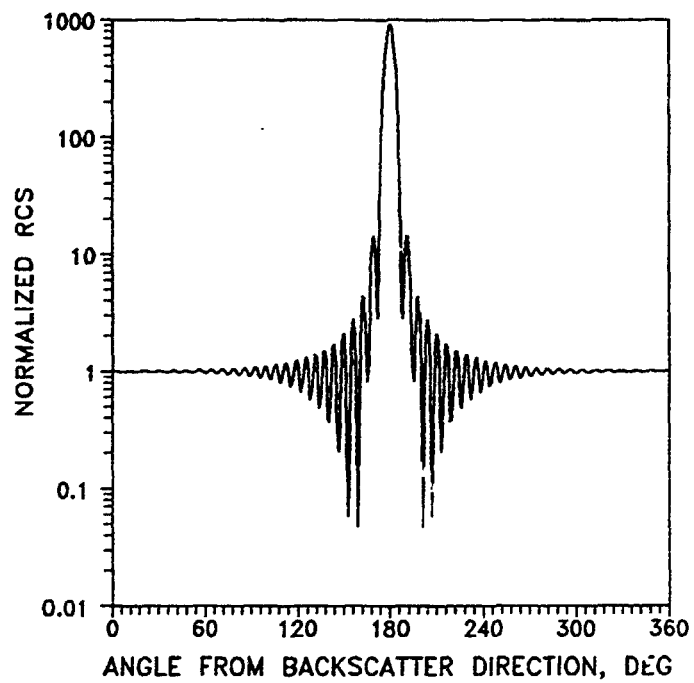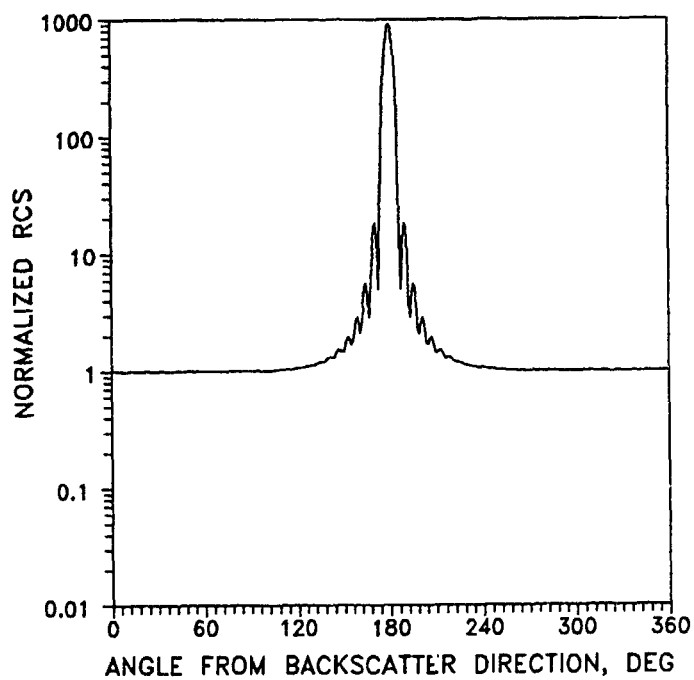
4

Figure 2. E-Plane Scattering From a Sphere



Figure 3. H-Plane Scattering From a Sphere

5

from transmitter-to-sphere-to-receiver. In particular,

$$E_1 \propto \sqrt{\sigma_1} \exp[j2k(d - l\cos\theta)] \tag{3}$$

and

$$E_2 \propto \sqrt{\sigma_2} \exp[j2k(d + l\cos\theta)] \tag{4}$$

where $d$ is the distance between the radar and the center of the dumbbell, $k = 2\pi/\lambda$ where $\lambda$ is the wavelength, $l$ is the half spacing of the spheres, and $\theta$ is the aspect angle. The RCS of the barbell is the magnitude squared of the ratio of the total field $E_T = E_1 + E_2$ suitably normalized by the incident field. Thus the monostatic RCS $\sigma_{TM}$ of the barbell is

$$\sigma_{TM} = |E_1 + E_2|^2 = \sigma_1 + 2\sqrt{\sigma_1 \sigma_2}\cos[4kl\cos\theta] + \sigma_2. \tag{5}$$

It is apparent that if $\sigma_1 = \sigma_2$, the maximum and minimum values of $\sigma_{TM}$ will be $4\sigma_0$ and 0 respectively. Also if $\sigma_1 \gg \sigma_2$, then, $\sigma_{TM} \approx \sigma_1$. Equation (5) is plotted in Figure 5 for a sphere spacing of 20 wavelengths and $\sigma_1 = 2\sigma_2$.

The bistatic cross section is similarly calculated with the help of Figure 6. Now,

$$E_1 \propto \sqrt{\sigma_{1B}} \exp[j2(d - l\cos\theta + d^1 - l\cos[\beta + \theta])] \tag{6}$$

and

$$E_2 \propto \sqrt{\sigma_{2B}} \exp[j2(d + l\cos\theta + d^1 - l\cos[\beta + \theta])] \tag{7}$$

where $\sigma_{1B}$ and $\sigma_{2B}$ are the bistatic cross section of the spheres and $d^1$ is the distance between the radar and the end of a sphere as shown in Figure 6. As before, the bistatic cross section of the dumbbell for $d = d^1$ is

$$\sigma_{TB} = |E_1 + E_2|^2 = \sigma_{1B} + 2\sqrt{\sigma_{1B}\sigma_{2B}}\cos[2kl(\cos\theta + \cos(\beta - \theta)] + \sigma_{2B}. \tag{8}$$

Inspection of Eq. (8) shows that $\sigma_{TB} = \sigma_{TM}$ for $\beta = 0°$.

Equation (8) is plotted in Figure 7 with $\sigma_{1B} = \sigma_1$ and $\sigma_{2B} = \sigma_2$ for a range of bistatic angles. It is apparent that as the bistatic angle increases the magnitude and frequency (direction changes per degree of aspect angle change) of the RCS fluctuations decrease steadily. It should be noted that had the correct values $\sigma_{1B}$ and $\sigma_{2B}$ been used in Equation (8), the curves would have shown the same trends but the mean RCS would have depended in the variation of $\sigma_{1B}$ and $\sigma_{2B}$ with bistatic angle.

## 2.3 Bistatic Radar Cross Section

Enhanced RCS and reduced fluctuation rates can provide a bistatic radar greater detection probabilities than an equivalent monostatic radar. Probability detection is a good estimation of the performance of a radar system and will be used here to compare monostatic and bistatic system performance.
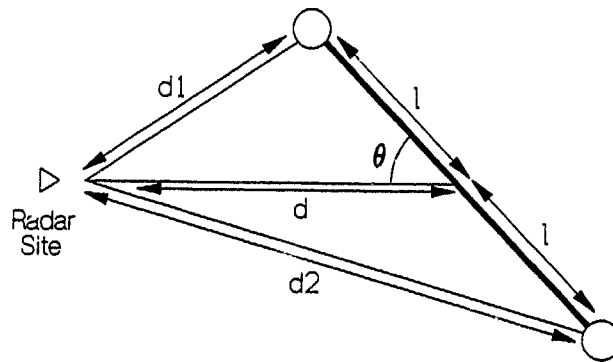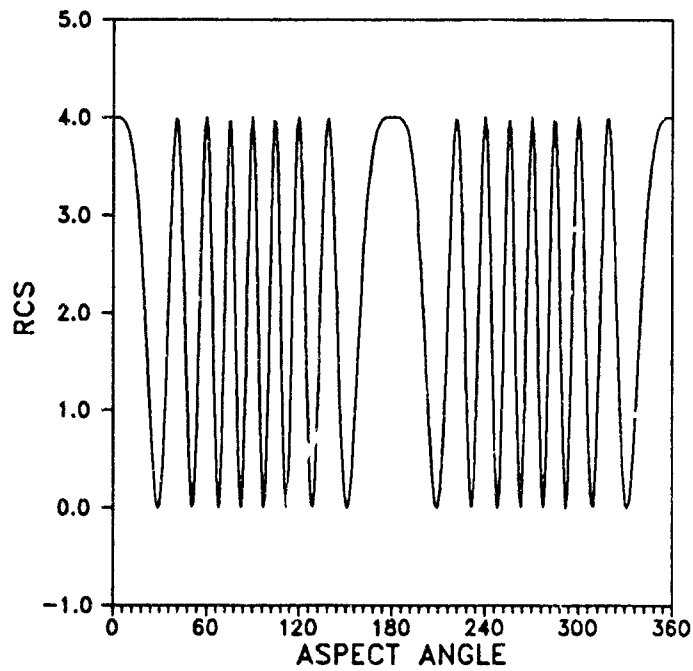
Figure 4. Monostatic Barbell Configuration



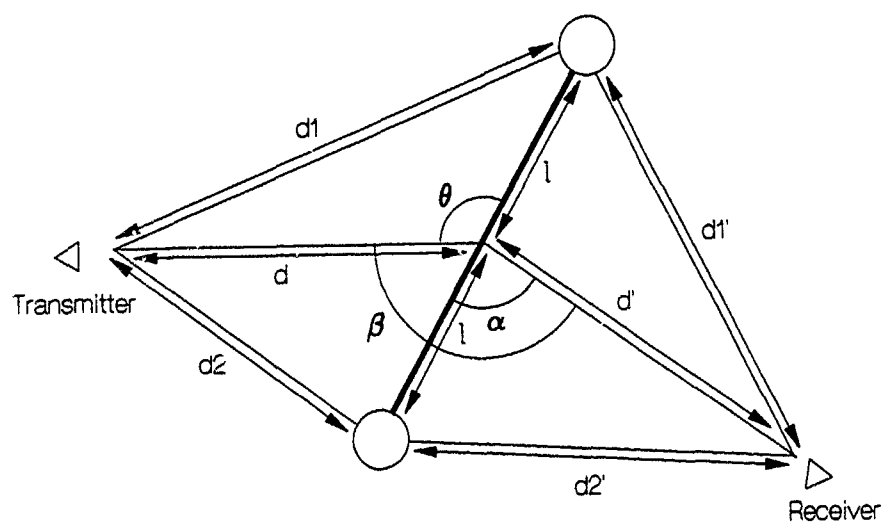Figure 5. Monostatic Barbell Fluctuations
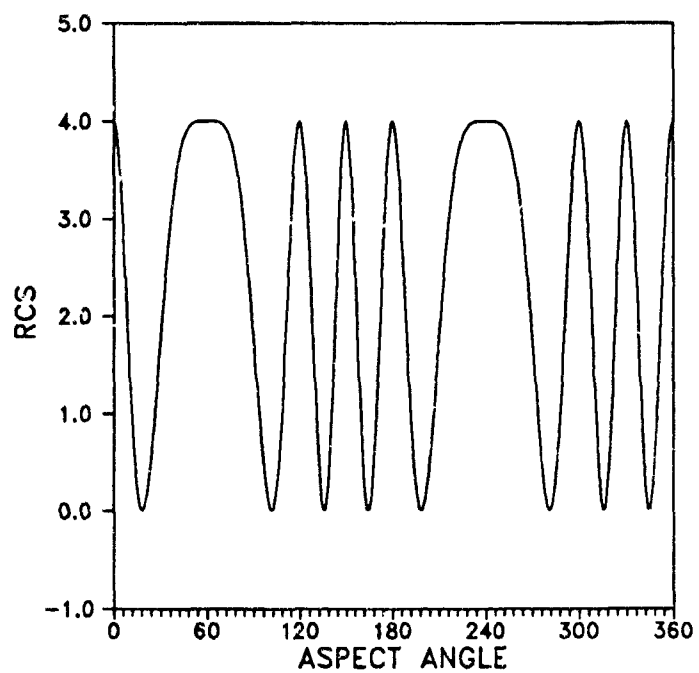
Figure 6. Bistatic Barbell Configuration



Figure 7. Bistatic Barbell Fluctuations

8

To perform this type of analysis for bistatic configurations, the bistatic RCS of a target is required. Bistatic measurements are extremely difficult to obtain for even the simplest shapes. As we are interested in a complete set of the bistatic RCS for a cylinder, (bistatic angles ranging from 0 − 180°), a computer simulation is used to determine the RCS for bistatic angles ranging from 0 − 180°. The RADC/Syracuse Research Corp. bistatic radar cross-section (BSRCRCS) computer program is used to obtain the RCS plots for the cylinder.[11]

### 2.3.1 RCS AMPLITUDE PLOTS

The computed RCS's of a 15-wavelength long, 2-wavelength-in-diameter cylinder are shown in Figures 9 to 17 for several bistatic angles. The plots show RCS as a function of the aspect angle $\theta_{az}$ defined in Figure 8. Comparison of the curves shows the increase in RCS and the reduction in the magnitude and rate of the fluctuations as the bistatic angle increases. These trends are generally observed for targets with characteristic dimensions much larger than a wavelength.

## 2.4 PDFs and Detection Theory

Radar detection depends upon both the returned signal from the target and the internal receiver noise. Both of these signals are continually varying and are modeled as random processes characterized by appropriate probability density functions (PDFs). A detection is declared whenever the voltage at the receiver output exceeds a specified threshold. When a detection is recorded and no target is present, a false alarm is said to have occurred. A false alarm is the consequence of the internal receiver noise (and clutter residue) exceeding the established detection threshold. If a target is present the threshold crossing is bona fide target detection. The probability density function for the noise signal alone and the desired probability of false alarm are used to calculate the threshold voltage. This voltage with the PDF for the noise plus target signal is then used to compute the probability of detection as a function of the signal power to noise power ratio.

A rigorous examination of the probability of detection is included in Section 5. For now the PDFs of the noise alone and the signal plus noise are used to describe how they characterize the detection process. Figure 18 shows how the PDFs of the signal and noise are related to the probability of detection. These PDFs are examples and are not the actual PDFs. Once the threshold level as detailed above is set, the probability of detection is the area under the signal-plus-noise PDF for abscissa greater than the threshold level. The probability of false alarm, $P_{fa}$, is also marked in the figure, and is the area under the noise voltage PDF for abscissa greater than the threshold level. This is the probability of mistaking noise for a target when no target is present.

Any changes in the signal-plus-noise PDF affects the probability of detection This report is aimed at determining how the enhanced RCS and reduced fluctuation rate observed in bistatic radar affect the PDFs. Figure 19 shows schematically the effect of reduced fluctuation rates and enhanced mean RCS on the PDF. From the figure it can be seen that a decrease in fluctuation rate causes the PDF to become narrower, and an increase in mean RCS amplitude causes the PDF to move to the right.

---

[11] Cha, C., Michels, J., and Starczewski, E. (1988) An RCS Analysis of Generic Airborne Vehicles Dependence Upon Frequency and Bistatic Angle, *Proceedings of the 1989 IEEE National Radar Conference* pp 214-219
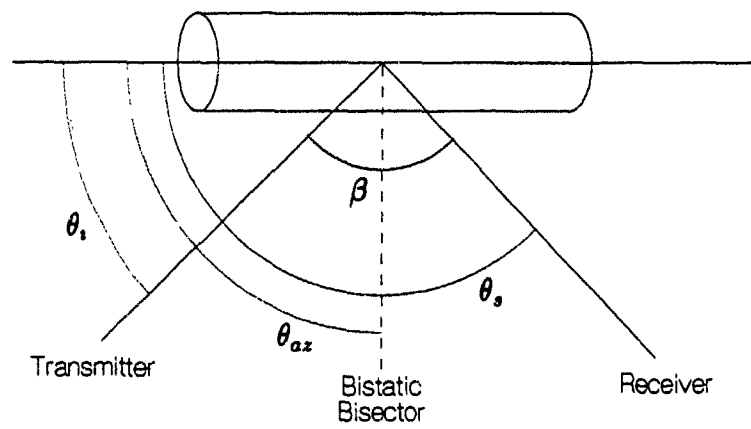
Figure 8. Bistatic Geometry



Figure 9. RCS Amplitude versus Aspect Angle for $\beta = 0°$

10

Figure 10. RCS Amplitude versus Aspect Angle for $\beta = 100°$



Figure 11. RCS Amplitude versus Aspect Angle for $\beta = 110°$

11

Figure 12. RCS Amplitude versus Aspect Angle for $\beta = 120°$



Figure 13. RCS Amplitude versus Aspect Angle for $\beta = 130°$

Figure 14. RCS Amplitude versus Aspect Angle for $\beta = 140°$



Figure 15. RCS Amplitude versus Aspect Angle for $\beta = 150°$
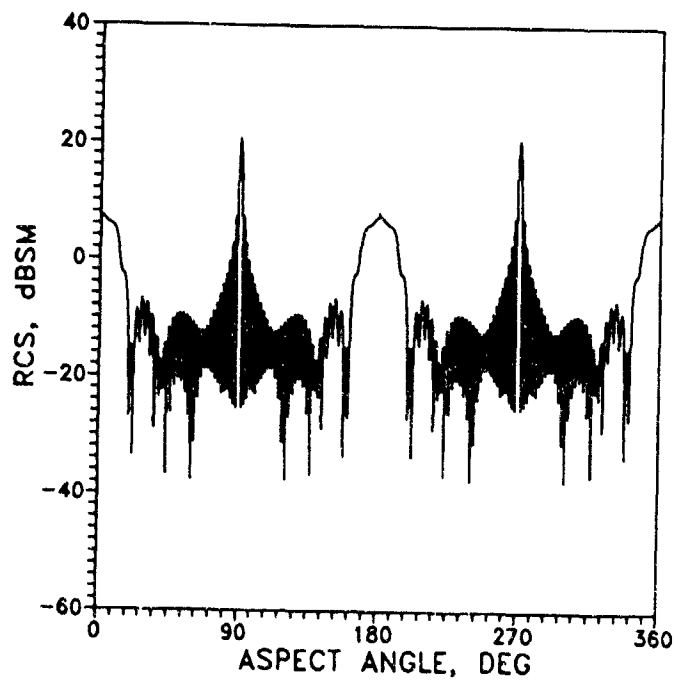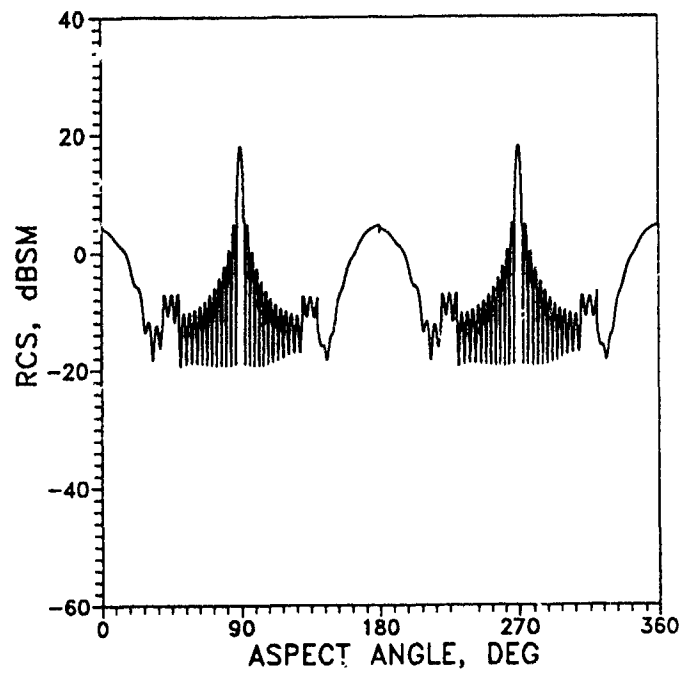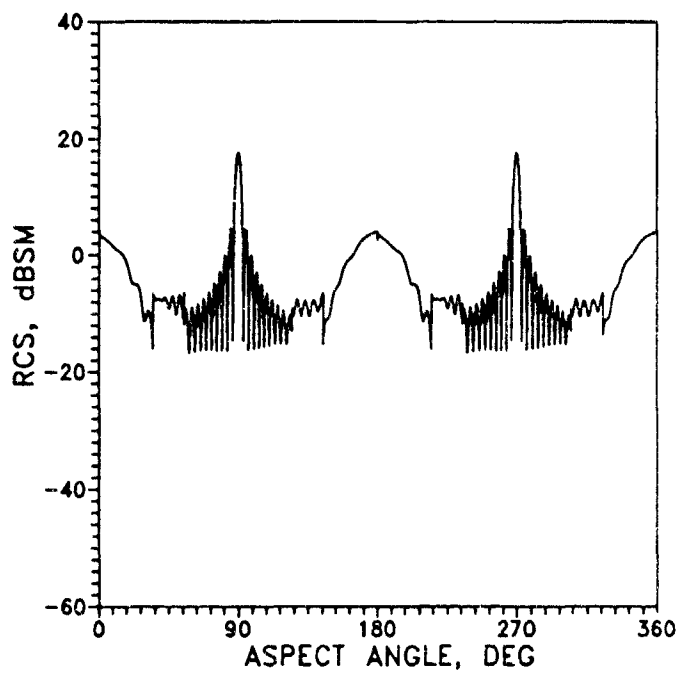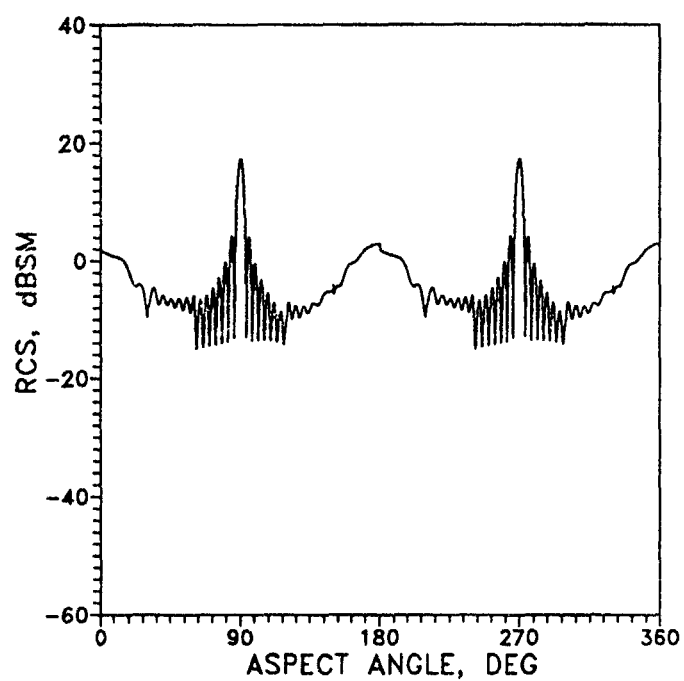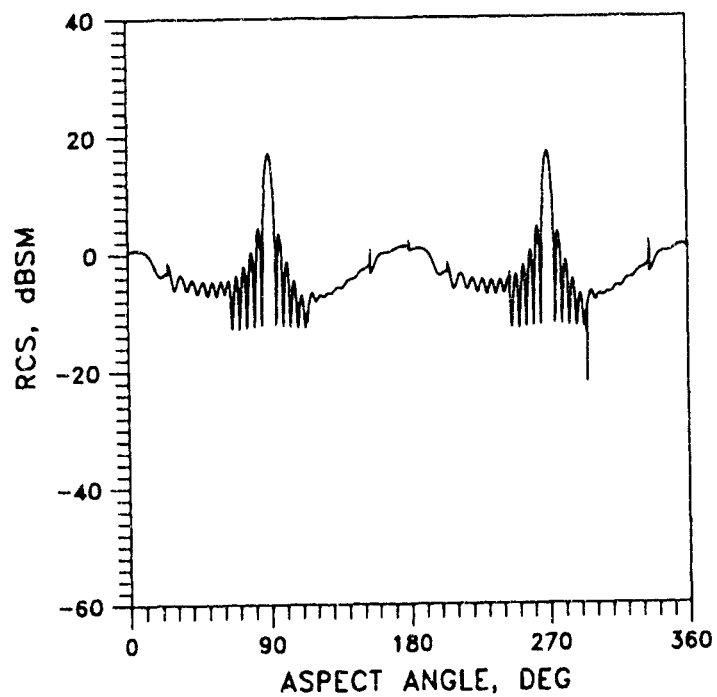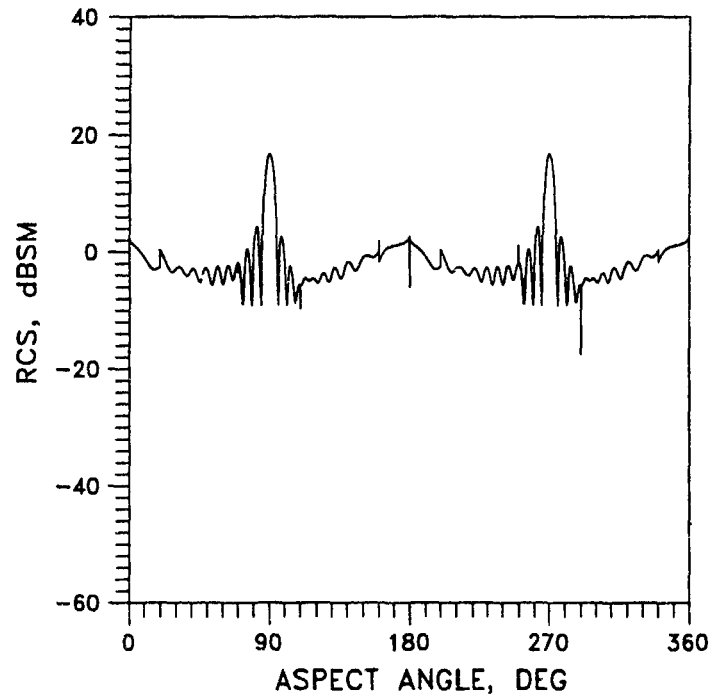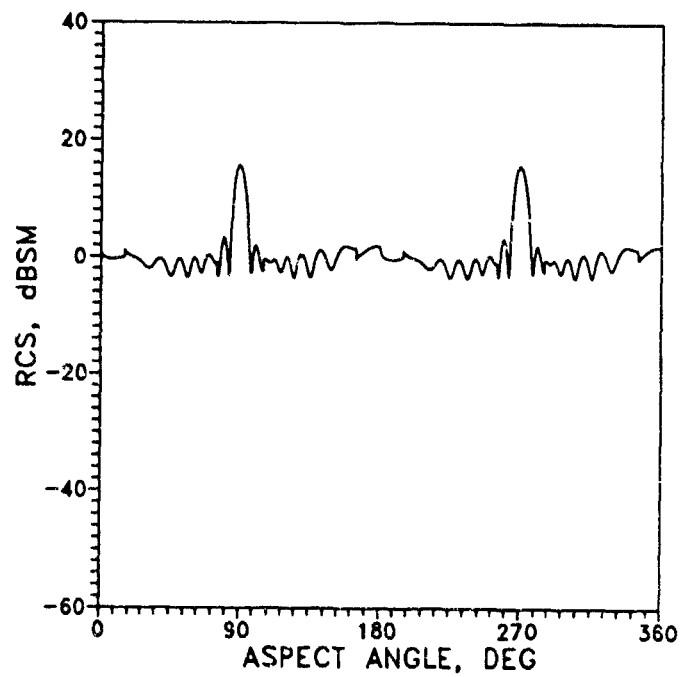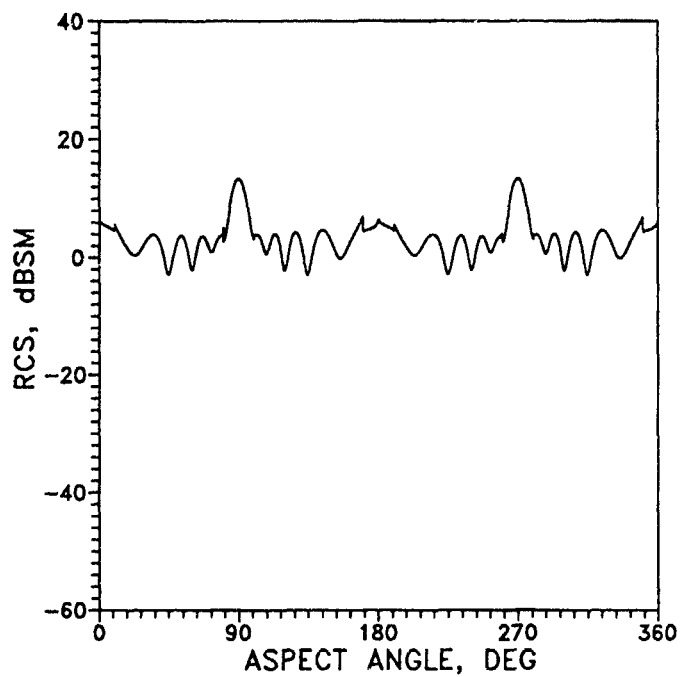
Figure 16. RCS Amplitude versus Aspect Angle for $\beta = 160°$
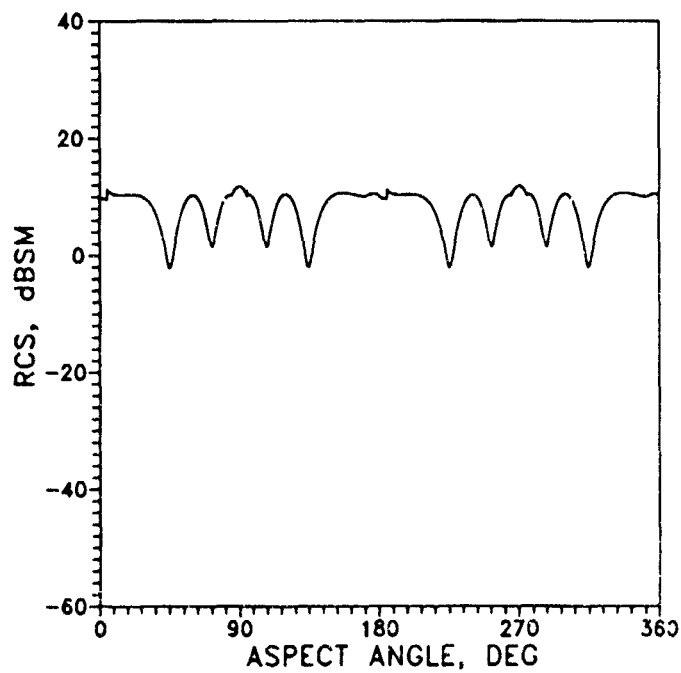


Figure 17. RCS Amplitude versus Aspect Angle for $\beta = 170°$
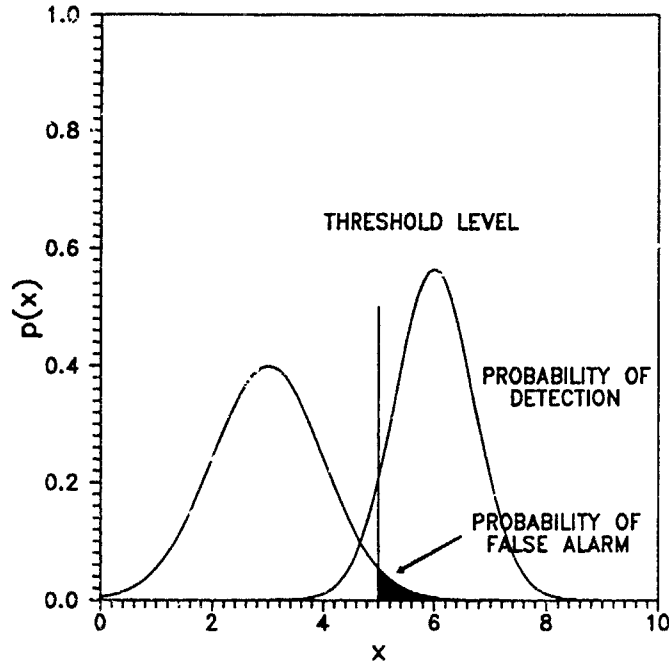
Figure 18. PDF and Probability of Detection

These changes in the PDF directly affect the probability of detection. Figure 20 shows the effect of reduced fluctuation rates and enhanced mean RCS on the probability of detection, $P_D$. Looking at Figure 20, we can see that if the probability of false alarm, $P_{fa}$, is held constant, then the probability of detection increases as the mean value of the RCS is increased. Conversely, the $P_{fa}$ can be decreased with the $P_D$ remaining constant or even increasing by raising the threshold.

The definition of the PDF $p(x)$ for a discrete random variable is defined as:

$$p(x) = \sum_i p_i \delta(x - x_i) \quad p_i = P(x = x_i) \tag{9}$$

where $p_i$ is the probability that $x = x_i$. In this analysis, $x$ is the RCS of the cylinder and $p_i = 1/i$. The PDFs of the cylinder RCS are found by setting range bins of RCS, $[\delta(x - x_i)]$ and determining the number of times the RCS falls within a given range bin. The number of 'hits' for each range bin is then divided by the total number of samples. Figures 21 through 29 show the PDFs for the cylinder RCS. The PDFs are computed for the entire range of aspect angles, $0 - 360°$, for the cylinder. The entire range is used in this analysis under the assumption of no knowledge of cylinder orientation relative to the radar.

From these figures, it is hard to discern the difference between the PDF's for the monostatic and bistatic cases. To show the increase in mean and the reduced fluctuation rates, Table 1 has the mean, variance and coefficient of variation, CV, for the various cases. The coefficient of variation is defined in Reference 12 as the ratio of the standard deviation to the mean; $CV = \sigma/\mu$. The standard deviation is a common measure of dispersion of a random variable. The coefficient of variation provides a measure of the
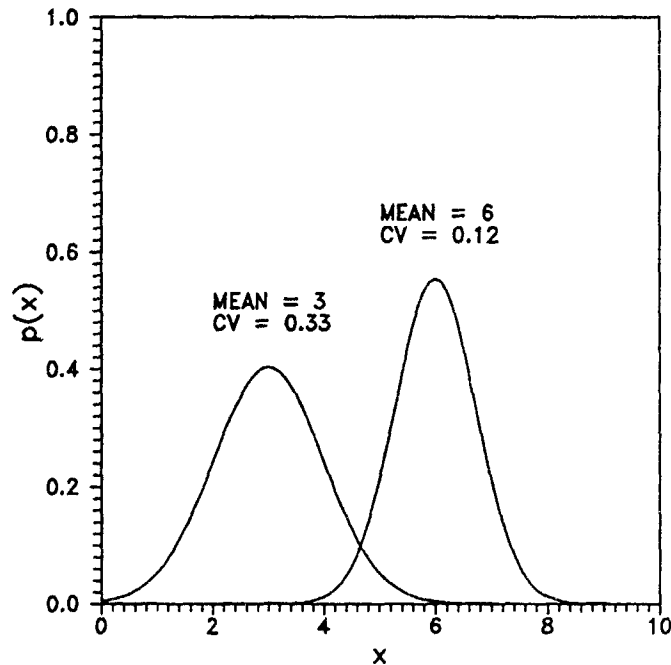
Figure 19. Effect of Increased Mean on PDF

variability normalized to the mean. The coefficient of variation is useful when comparing the variability of these data sets of RCS because they differ in the magnitude of the observations as the bistatic angle is increased.

The coefficient of variation is used as a measure of the reduced RCS fluctuation rate. As the fluctuation rate decreases, so will the coefficient of variation. From Table 1, the increase in mean, normalized and unnormalized, is clear, and the reduced variability is shown by the decrease in the coefficient of variation with increasing bistatic angle.

## 3   THEORY OF RCS SCATTERING

Statistical descriptions of the RCS and the noise processes are necessary for estimating radar system performance. The noise processes are the limiting factor in radar detection and are dealt with in depth in Section 4. Given the simulated bistatic RCS distributions, it is worthwhile to determine a closed form distribution that will provide an accurate description of the RCS. A closed form description of the bistatic RCS distributions allows for the evaluation and comparison of the detection probabilities for both the monostatic and the bistatic cases.

Several statistical target models have been used to describe various fluctuating target cross sections. Swerling's two fluctuating models have probably been the most widely used as they apply reasonably well to a variety of targets.[12]  With the development of large, high

---

[12] Swerling, P (1960) Probability of Detection for Fluctuating Targets, *IRE Trans. Inform. Theory*, IT-6:65-217.

Figure 20. Effect of Increased Mean on $P_D$

Table 1. Cylinder Statistics, Horizontal Polarization

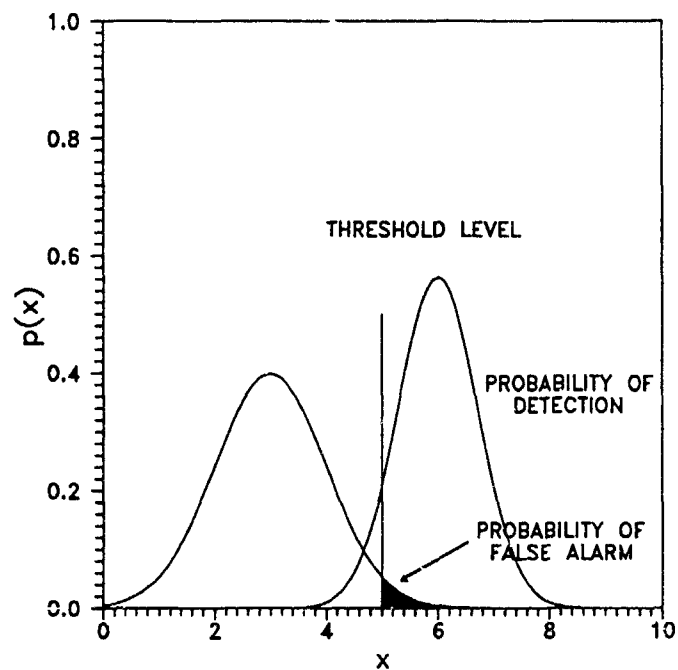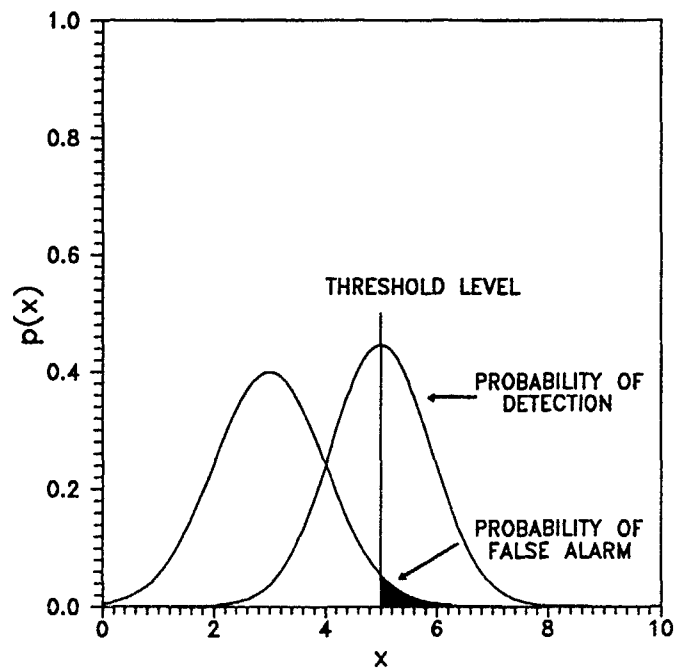| Bistatic Angle | Unnorm Mean (sm) | Norm Mean | Variance | CV |
|---|---|---|---|---|
| 0° | 1.7969 | 0.0157 | 0.0069 | 5.2908 |
| 100° | 1.4997 | 0.0232 | 0.0107 | 4.4587 |
| 110° | 1.4990 | 0.0256 | 0.0119 | 4.2612 |
| 120° | 1.5652 | 0.0286 | 0.0136 | 4.0776 |
| 130° | 1.6987 | 0.0319 | 0.0159 | 3.9528 |
| 140° | 1.9389 | 0.0411 | 0.0191 | 3.3626 |
| 150° | 2.2019 | 0.0596 | 0.0238 | 2.5885 |
| 160° | 2.9434 | 0.1309 | 0.0293 | 1.3077 |
| 170° | 7.8533 | 0.2703 | 0.0202 | 0.5258 |

speed computers, the use of other distributions has become simpler. It has been shown [13] that the beta distribution can provide a more accurate target model for the monostatic RCS for complex targets. In our analysis it has been determined that the beta distribution provides the best description of the monostatic and bistatic RCS of the cylinder and is used in the determination of detection probabilities for the cylinder.

## 3.1 Use of The Beta Distribution

Three statistical parameters are used to describe variation of RCS with aspect and bistatic angle. These parameters are determined from combinations of moments about the mean RCS and are used to find an appropriate characterizing distribution for the bistatic RCS. The parameters are

**Width,** $w = m_2/m^2$ where m is the mean, and $m_2$ is the second moment about the mean; the variance,

**Modified Skewness,** $g = m_3/m_2 m$ where $m_3$ is the third moment about the mean, and

**Kurtosis,** $K = m_4/m_2^2 - 3$ where $m_4$ is the fourth moment about the mean.

The location of calculated points in the width-skewness plane allows us to determine which distribution provides the best description of the data. Figure 30 shows the locations of several distributions in the $(w, g)$ plane.

The area below the line $g = w - 1$ is nonphysical, that is, there exists no nonnegative probability distribution of positive quantities that can place a point $(w, g)$ in this region. The general chi–square model is represented by the line $g = 2w$, which contains the Swerling models, including the Rayleigh point. The log–normal distribution is represented by the line $g = w(w + 3)$. These lines represent the various $(w, g)$ points as the shape parameters of the chi–square and log–normal distributions are varied.

The $(w, g)$ values for a complex target can lie anywhere within the region defined below $g = 2w$ and above $g = w - 1$ in Figure 30.[14] The chi–square, log–normal, and Rayleigh

---

[13] Follin, J.W., Paddison, F C., and Maffett, A.L. (1984) Statistics of Radar Cross Section Scintillations, *Journal of Electromagnetics*, 4:139-164

[14] Follin, J.W., Paddison, F.C., and Maffett, A.L. (1984) Statistics of Radar Cross Section Scintillations, *Journal of Electromagnetics*, 4:139-164.

Figure 21. Cylinder PDF For $\beta = 0°$

Figure 22. Cylinder PDF For $\beta = 100°$

Figure 23. Cylinder PDF For $\beta = 110°$
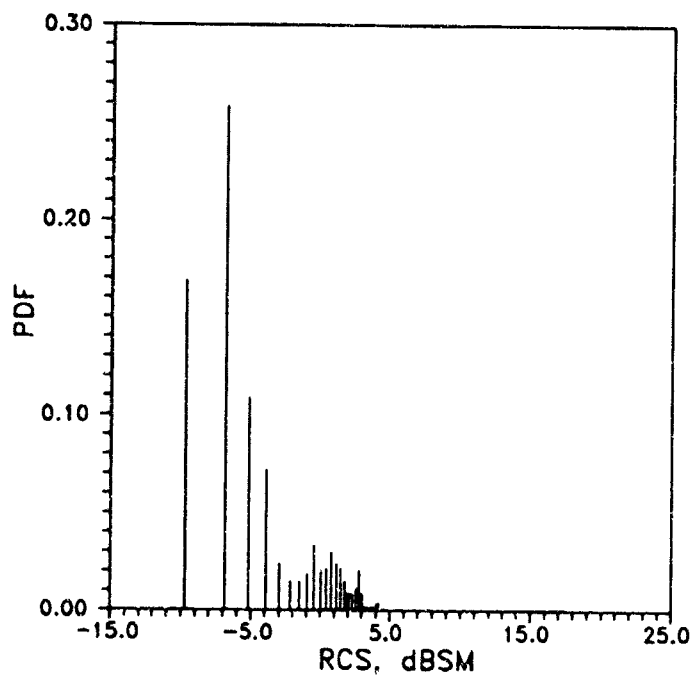


Figure 24. Cylinder PDF For $\beta = 120°$
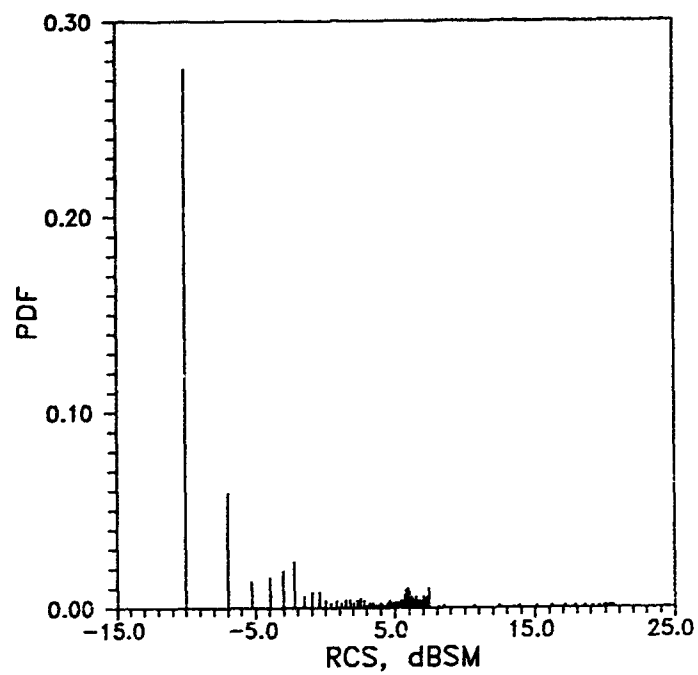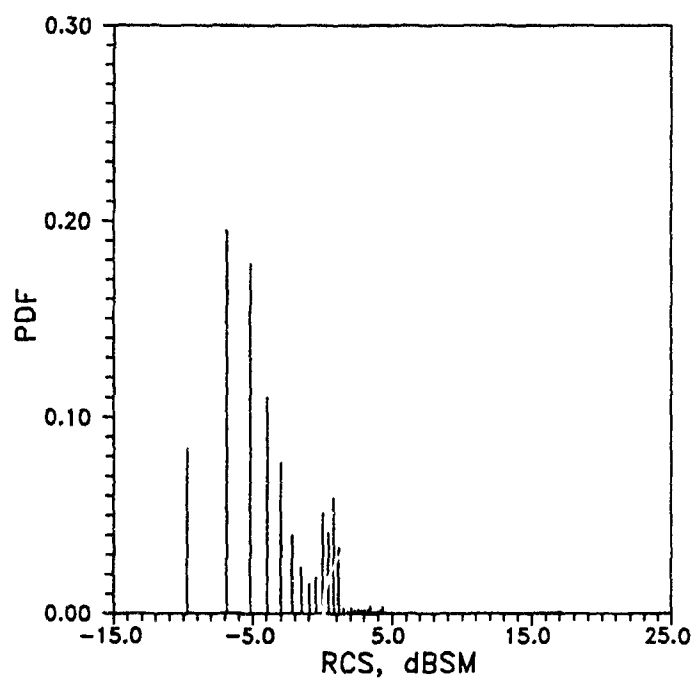
Figure 25. Cylinder PDF For $\beta = 130°$
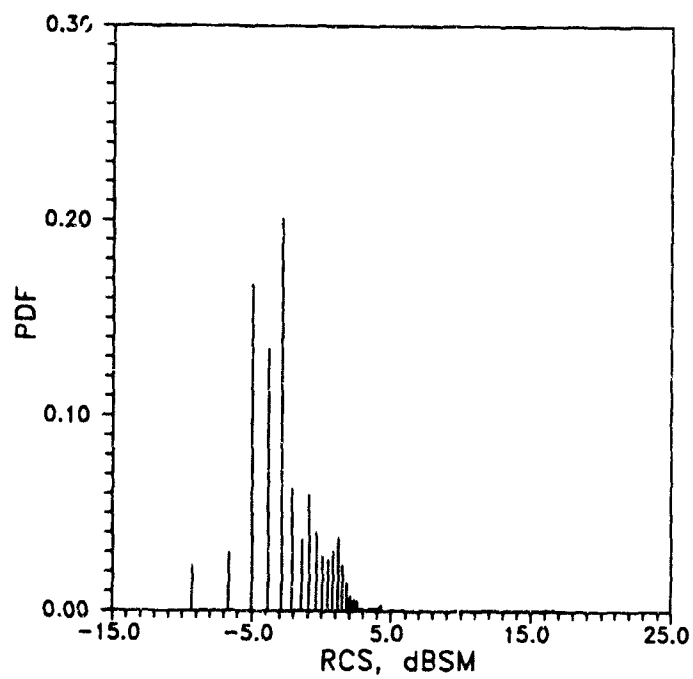


Figure 26. Cylinder PDF For $\beta = 140°$
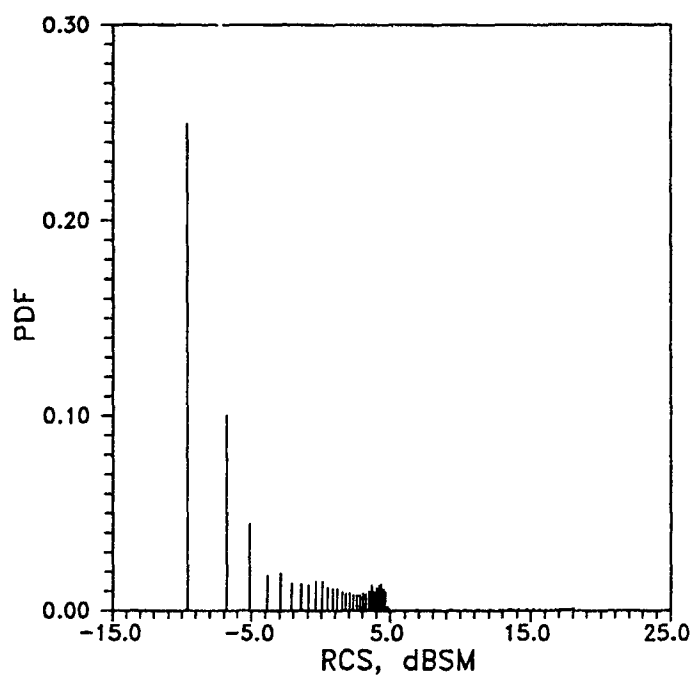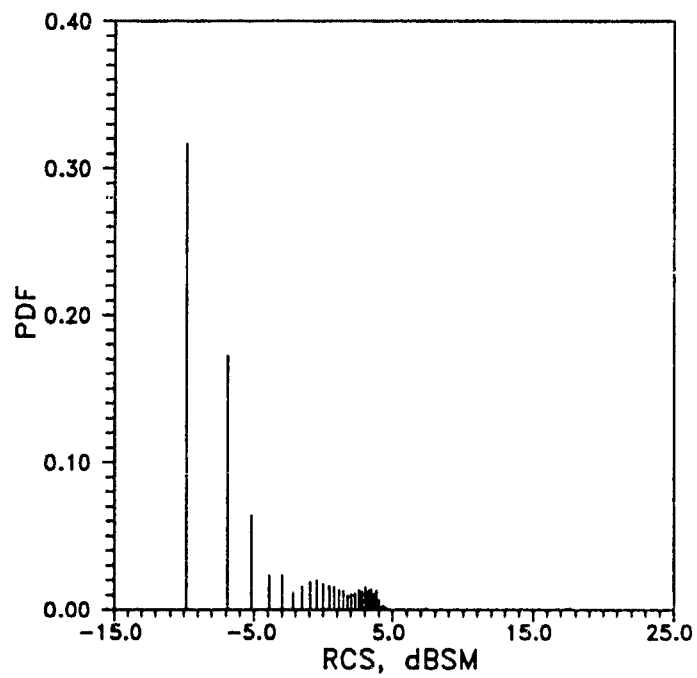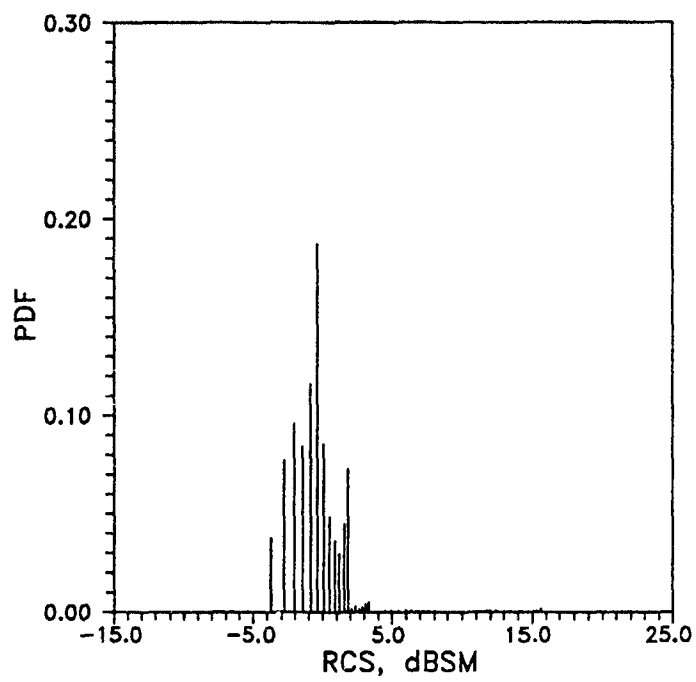
Figure 27. Cylinder PDF For $\beta = 150°$
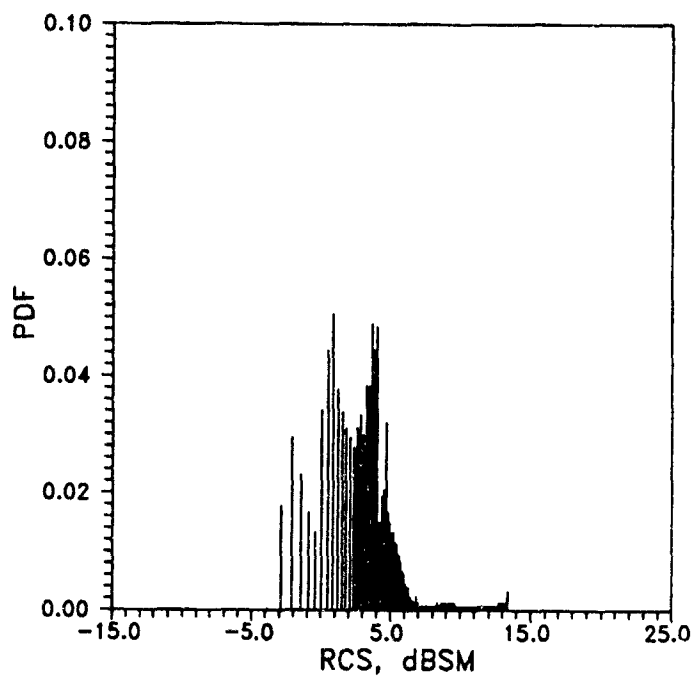


Figure 28. Cylinder PDF For $\beta = 160°$

22
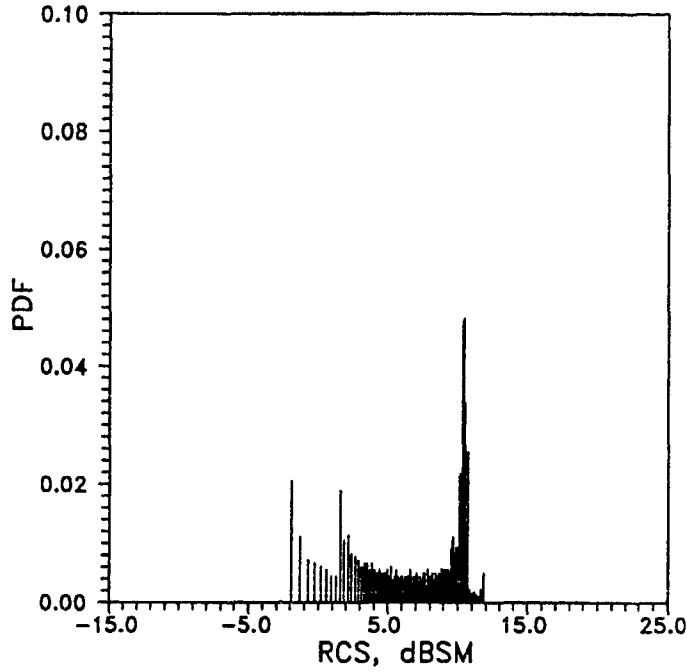
Figure 29. Cylinder PDF For $\beta = 170°$

distributions all lack the statistical flexibility to span the area, for the $(w, g)$ points are well defined by the $\chi^2$ family line shown. Thus we can see that for these distributions to be an accurate model for a sample, the $(w, g)$ point of the sample must lie close enough to the $(w, g)$ curve of the distribution. We find, however, that the beta distribution spans the entire area above the line $g = w - 1$ up to $g = 2w$. This allows us to fit a beta distribution to any sample distribution for a complex target, that is, we are guaranteed to have a distribution that will either include or lie extremely close to the $(w, g)$ point of the sample distribution. It is this flexibility that makes the beta distribution very useful as a fluctuation model for complex targets.

## 3.2 Beta Distribution

The beta distribution is defined as

$$\beta(x : a, b) = \frac{\Gamma(a + b)}{\Gamma(a)\Gamma(b)} x^{a-1}(1 - x)^{b-1}, \quad a, b > 0, \quad 0 \le x \le 1, \tag{10}$$

where the parameters $a$ and $b$ determine the specific shape of the beta distribution. The flexibility of the beta distribution arises from the fact that it is a two parameter distribution. Note that the beta distribution is defined from 0 to 1. We therefore develop a normalized form for the RCS represented by $x$ such that $0 \le x \le 1$ using $x = \frac{\sigma - \sigma_{min}}{\sigma_{max} - \sigma_{min}}$ where $\sigma_{min}$ and $\sigma_{max}$ are the minimum and maximum values of the RCS $\sigma$ respectively.

The shape parameters $a$ and $b$ are computed from the first four moments about the mean. First determine $n$ and $p$, defined as,

23
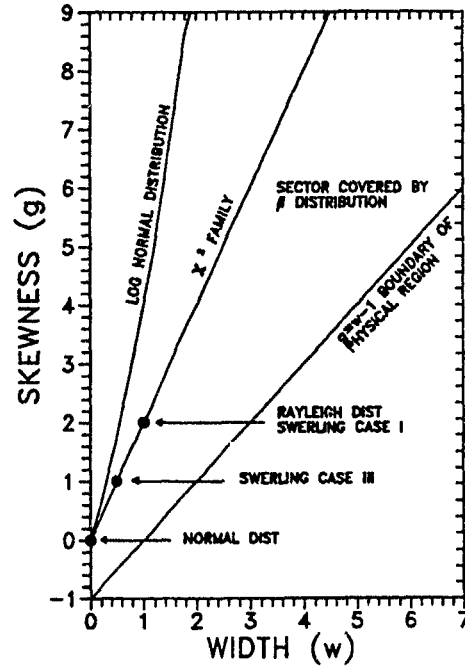
Figure 30. Width-Skewness Plane

$$n = \frac{g+2}{2w-g} \quad , \quad \text{and} \quad p = \frac{1}{nw} \quad . \tag{11}$$

Solving $n = a + b + 1$ and $p = a/b$ for $a$ and $b$, we get

$$a = \frac{p(n-1)}{p+1} \quad , \quad \text{and} \quad b = \frac{n-1}{p+1} \quad . \tag{12}$$

Appendix A contains tables of these parameters for the cylinder RCS distributions for various configurations and polarizations.

## 3.3 CDF Plots

The cumulative distribution function (CDF) provides a method for showing the goodness of fit of the beta distribution to the bistatic RCS distributions of the cylinder. The chi-squared, with two and four degrees of freedom, and the log-normal distributions are shown for comparison. The CDF plots are taken over the entire range of aspect angle, $0 - 360°$. Figures 31 thru 38 show these plots for the monostatic and various bistatic angles. All the plots shown are for horizontal polarization. For the CDF plots the abscissa is normalized to ensure that the mean of the cylinder data and the mean of the beta distribution are equal. This normalization is as follows;

$$\text{Abscissa} = (\frac{a}{a+b}) \times \frac{\text{RCS}}{\text{mean}} .$$

24

The CDF plot for the bistatic angle of 160° is not included as we are unable to fit a beta distribution to the data. It is possible that the statistics of the data do not lie within the region of coverage for the beta distribution, as is the case for the cylinder when the bistatic angle is 160° and the aspect angle range is 0 − 360°.

### 3.3.1 KOLMOGOROV–SMIRNOV TWO SIDED TEST

The CDF plots of the data and distribution functions are used to measure how well they fit the data. The Kolmogorov–Smirnov two–sided test is used as the measure of the goodness of the fit. This test uses the maximum deviation of the theoretical CDF from the empirical CDF. Based upon certain quantiles, we will have the maximum deviation necessary for a theoretical CDF to be considered an accurate description of the empirical CDF. Applying this test allows us to determine which distribution provides the most accurate description of the cylinder RCS.

The Kolmogorov–Smirnov two–sided test was applied with a 0.98 percentile which gives[15] a maximum deviation of 0.215, for N = 100 data points. Thus the probability is 0.98 that the largest absolute deviation of two CDF's is 0.215 or less when N = 100.

To provide an adequate fit to the empirical CDF, a theoretical CDF must have a maximum deviation no greater than 0.215. The cylinder RCS data and other distribution functions were tested using this criteria for various bistatic angles and sectors of aspect angle; that is 10°, 20°, 30°, ... sectors. When applied, it is found that for approximately 90 percent of the cases the beta CDF yields a maximum deviation less than 0.215. Compare this to 10 percent for the chi–squared with two degrees of freedom, 14 percent for the chi–squared with four degrees of freedom, and 28 percent for the log–normal distribution. Table 4 contains the K–S statistics for the various bistatic angles with horizontal polarization and Table 5 contains the K–S statistics for the vertical polarization case. These statistics are computed for the entire aspect angle range, 0 − 360°. These tables are included in Appendix B.

Through the use of the Kolmogorov–Smirnov two–sided test, it is found that the beta distribution provides the best description of the cylinder RCS for both the monostatic and bistatic cases. These findings are in accordance with previous work with the beta distribution.[16] For these reasons the beta distribution is used as the fluctuation model in the determination of detection probabilities for both the monostatic and bistatic configurations.

## 4  PROBABILITY OF DETECTION

Marcum and Swerling developed the first widely used methods in the determination of detection probabilities for signals in noise.[17,18] Marcum completed work in this area where the signal from the target was constant. Swerling extended Marcum's work to include fluctuating signals. In this work, Swerling used four models to classify the fluctuating

[15] Daniel, W.W. (1978) *Applied Nonparametric Statistics*, Houghton Mifflin Co., Boston, MA.

[16] Follin, J W , Paddison, F.C., and Maffett, A.L. (1984) Statistics of Radar Cross Section Scintillations, *Journal of Electromagnetics*, 4:139-164

[17] Marcum, J I (1960) A Statistical Theory of Target Detection by a Pulsed Radar, *IRE Trans. Inform Theory*, IT-6. 145-267.

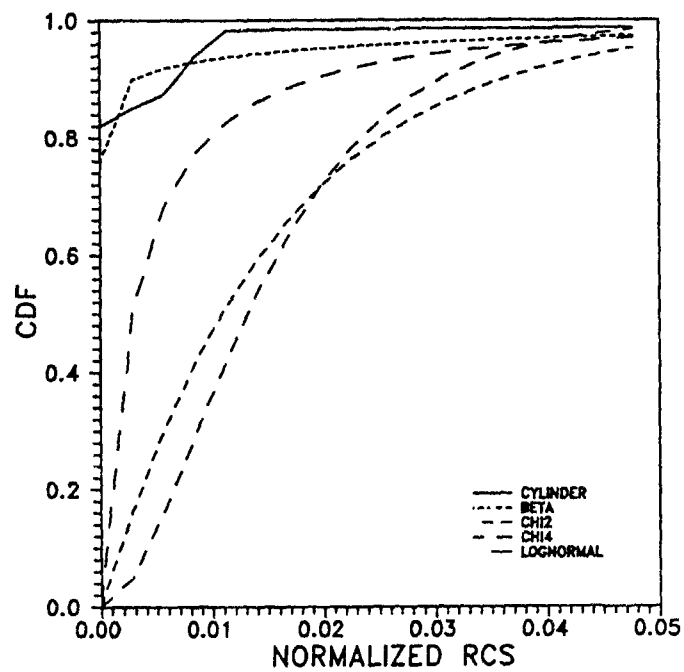[18] Swerling, P. (1960) Probability of Detection for Fluctuating Targets, *IRE Trans. Inform. Theory*, IT-6.65-217.

Figure 31. CDF Plot for Monostatic Case



Figure 32. CDF Plot for $\beta = 100°$

26

Figure 33. CDF Plot for $\beta = 110°$



Figure 34. CDF Plot for $\beta = 120°$

27

Figure 35. CDF Plot for $\beta = 130°$
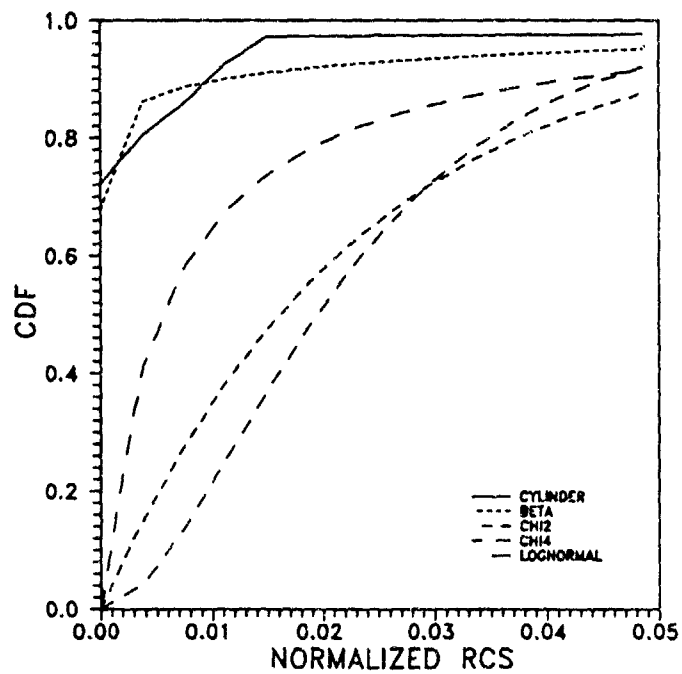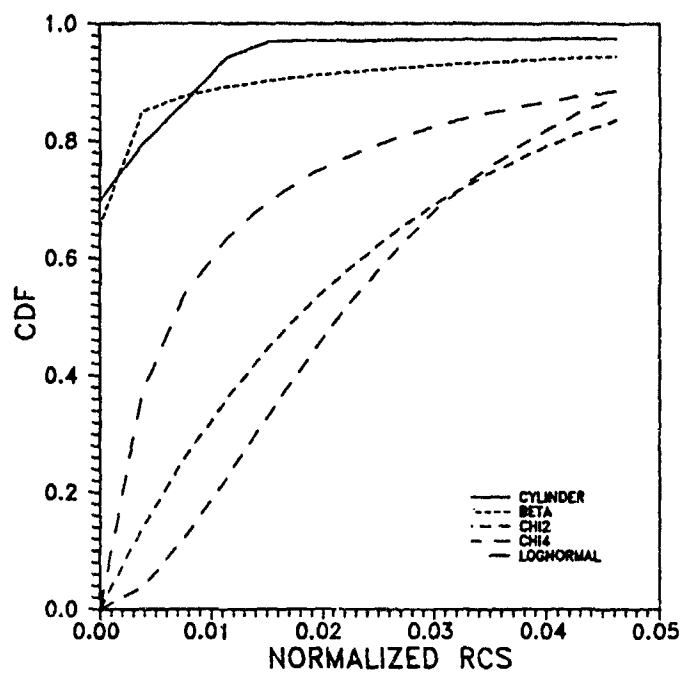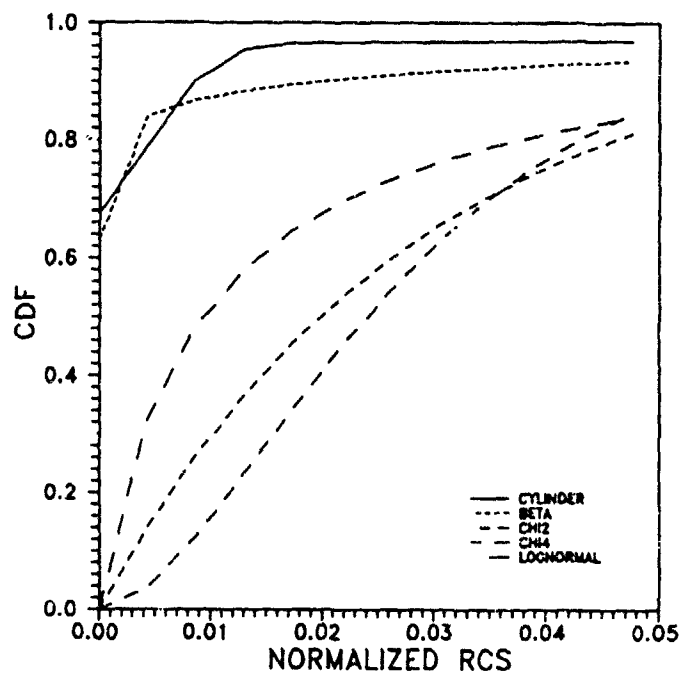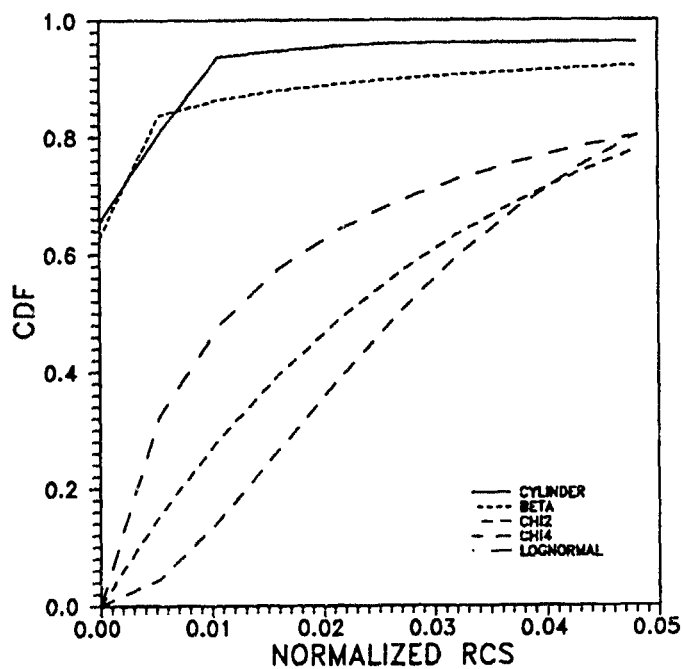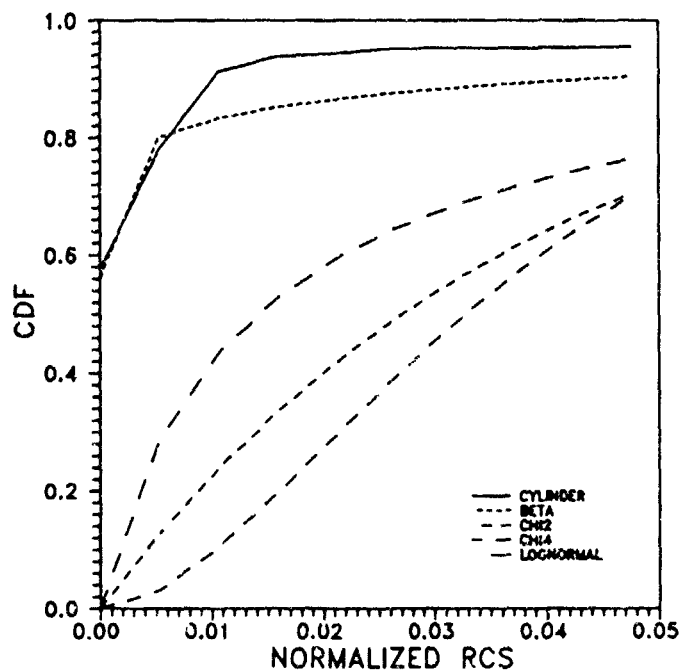


Figure 36. CDF Plot for $\beta = 140°$
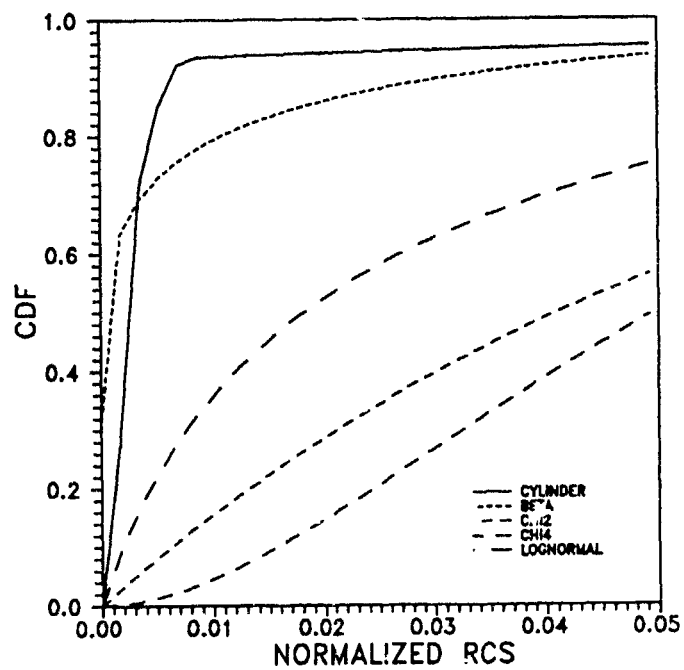
Figure 37. CDF Plot for $\beta = 150°$
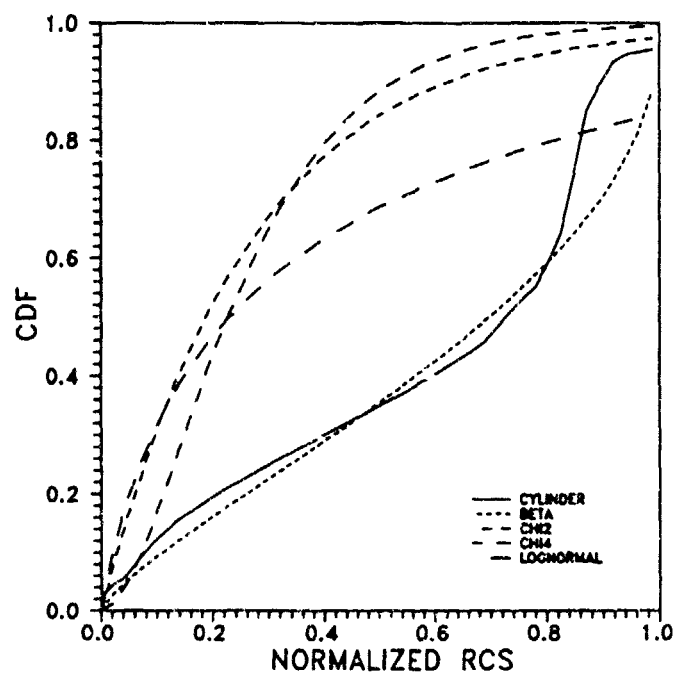


Figure 38. CDF Plot for $\beta = 170°$

Signal → RF Amp → Mixer → IF Amp → Detector → Integrator → Display

LO (connected to Mixer)
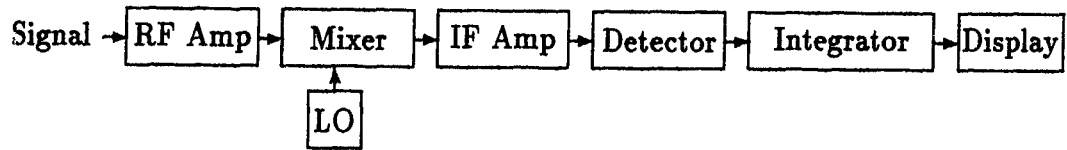
Figure 39. Radar Receiver Configuration

signals from targets. With the advent of large computers, other fluctuation models can readily be used in detection theory.

The focus of this work is on the detection probabilities for the beta distribution. It is helpful to begin with some elementary signal processing aspects of the radar receiver when going through the derivation of detection probabilities of signals in noise. Thus, we will briefly discuss the configuration of the typical radar receiver, the methods used to determine the probability of detection, and finally the probability of detection for the beta distribution.

## 4.1 Radar Receiver

The return signal from a target is processed by the radar receiver. The receiver amplifies and filters the echo signal to provide discrimination between the target signal and other interfering signals. The various processing that occurs in a receiver depends upon the application of the radar. In our discussion, we look at the receiver of a pulse type radar; one that transmits a burst of energy and listens for echoes between transmissions.

Most receivers are the superheterodyne type, shown in Figure 39. The incoming signal is shifted to an intermediate frequency (IF) by mixing with a local oscillator (LO) frequency. At the IF, the necessary filtering and amplification is easier to achieve. Filtering is the principal means by which the receiver discriminates between the echo signal and noise. The most effic'ent filter for discriminating between Gaussian noise and desired echoes is a matched filter. A matched filter is a passive network whose frequency response is the complex conjugate of the transmitted spectrum.

A square-law or linear detector can be used in the receiver. A square-law detector is assumed in the calculations of signal-to-noise ratio for detection probabilities. Three reasons for using a square-law detector are as follows:

1. Square-law detector is slightly superior to linear law detector for many-pulse integration.

2. Mathematical analysis is simpler for square-law detector.

3. Difference in performance of detectors is small.

Although a square-law detector is best for theoretical analyses, it is not used in practical radar.

The outputs of the detector are summed by a post-detection integrator. Many pulses

are returned from any particular dwell, and the integration of these return pulses can be used to increase the S/N ratio and improve detection accuracy. The integrated pulses are compared to a threshold level to determine the probability that a target is present. The integration can be accomplished either before or after the second detector.

Integration before the second detector is coherent integration while noncoherent integration is accomplished after the detector. The phase information from the signal is utilized in coherent integration. The phase information is destroyed by the detector, and noncoherent integration does not utilize this information. Also, the nonlinear action of the detector converts some of the signal energy to noise energy in the rectification process resulting in a loss of integration efficiency. Thus, coherent integration is more efficient but is more difficult to implement. Noncoherent integration is assumed for this analysis.

## 4.2 Detection Theory

Radar detection theory began with Marcum's work on the computation of detection probabilities for the nonfluctuating target in random noise using the aforementioned receiver configuration.[19] Swerling extended Marcum's work to include fluctuating targets.[20] The methods implemented by Marcum and Swerling have held as the standard method in the determination of detection probabilities for various distributions. This section reviews the methods used for determining the detection probabilities.

Assume that the noise from the receiver, entering the IF filter is Gaussian, with probability density function

$$p(V) = \frac{1}{\sqrt{2\pi\psi_o}} \exp\left(\frac{-V^2}{2\psi_o}\right) , \tag{13}$$

where V is the noise voltage, with variance $\psi_o$. When Gaussian noise is passed through a narrowband IF filter, the probability density function of the envelope of the noise voltage output is

$$p(R) = \frac{R}{\psi_o} \exp\left(\frac{-R^2}{2\psi_o}\right) , \tag{14}$$

where $\psi_o$ is the mean square value (or variance for a zero-mean process) of the noise voltage, and R is the voltage amplitude of the output envelope.

If the input to the filter contains a sine wave of amplitude S, as well as noise, then the probability density function, PDF, of the output of the square–law detector is

$$p(R) = \frac{R}{\psi_o} \exp\left[-\left(\frac{R^2 + S^2}{2\psi_o}\right)\right] I_o\left(\frac{RS}{\psi_o}\right) , \tag{15}$$

where $I_o$ is the modified Bessel function of zero order.

---

[19] Marcum, J.I. (1960) A Statistical Theory of Target Detection by a Pulsed Radar, *IRE Trans. Inform. Theory*, IT-6: 145-267

[20] Swerling, P (1960) Probability of Detection for Fluctuating Targets, *IRE Trans. Inform. Theory*, IT-6:65-217

If $v$ is the normalized amplitude of the envelope, $\frac{R}{\sqrt{\psi_o}}$ and $y$ is the output of the detector,

$$y = f\left(\frac{R}{\sqrt{\psi_o}}\right) = F(v) \,.$$

(16)

Letting $a = (S/\sqrt{\psi_o})$, we get

$$p(v) = v \exp\left[-\left(\frac{v^2 + a^2}{2}\right)\right] I_o(av).$$

(17)

Using a square law detector, we make the transformations, $y = (v^2/2)$ and $x = (a^2/2)$, where $x$ is the ratio of the average IF signal power to the average IF noise power. This now yields

$$p(y) = e^{-y-x} I_o(2\sqrt{xy}).$$

(18)

This is the conditional probability $p(y|x) = e^{-y-x} I_o(2\sqrt{xy})dy$. The characteristic function is determined from Campbell and Foster[21] as

$$C_1(p) = e^{-x}\left(\frac{\exp[x/(p+1)]}{p+1}\right)\,.$$

(19)

In the case of fluctuating targets, $x$ is a random variable with density function $w(x)$. The probability of a signal plus noise voltage sample having an amplitude $y$ after detection is given by Bayes' theorem as the conditional probability of having an amplitude $y$ given that the signal-to-noise ratio is $x$, times the probability that the signal-to-noise ratio was $x$.

$$\Rightarrow p(y,x) = p(y|x) \cdot w(x)$$

(20)

$p(y|x)$ is the single pulse density function given that the target has an echoing area that produces $x$, and $w(x)$ is the probability of having a target that yields a signal-to-noise ratio $x$. We determine the average single pulse density function, which is the average distribution of the ensemble.

$$E[p(y|x)] = \int_{-\infty}^{\infty} p(y|x)w(x)dx$$

(21)

$$= \int_{-\infty}^{\infty} p(y,x)dx \equiv g(y)\,,$$

(22)

where $g(y)$ is the marginal distribution of $y$.

---

[21] Campbell, G.A. and Foster, R.M. (1947),*Fourier Integrals for Practical Applications*, Van Nostrand Reinhold, Princeton, New Jersey.

The characteristic function associated with this average target is

$$\overline{C_1}(p) = \int_{-\infty}^{\infty} e^{py}g(y)dy = \int_{-\infty}^{\infty} e^{py}\left\{\int_{-\infty}^{\infty} p(y|x)w(x)dx\right\}dy \tag{23}$$

$$= \int_{-\infty}^{\infty} w(x)\left\{\int_{-\infty}^{\infty} e^{py}p(y|x)dy\right\}dx. \tag{24}$$

Now $\int_{-\infty}^{\infty} e^{py}p(y|x)dy = C_1(p)$, the characteristic function of y- the normalized post detector voltage arising single dwell, but to fluctuate independently from dwell to dwell. The fast fluctuating case, or pulse-to-pulse fluctuating, occurs when the fluctuations are independent from pulse to pulse. For a fast fluctuating target, the PDF of the detector output for N noncoherently integrated pulses is found by convolving the PDF for a single pulse with itself N-1 times. Thus, $\overline{C_N}(p)_{fast} = [\overline{C_1}(p)_{slow}]^N$.

Now the probability of detection can be arrived at by taking the inverse Laplace transform of the characteristic equations and integrating over y from $y_B$ to $\infty$, where $y_B$ is the threshold level. Thus,

$$P_D = \int_{y_B}^{\infty} \mathcal{L}^{-1}\left[\overline{C_N}(p)\right]dy = 1 - \int_{0}^{y_B} \mathcal{L}^{-1}\left[\overline{C_N}(p)\right]dy. \tag{25}$$

This method for the determination of detection probabilities is widely used.

## 4.3 Detection Probabilities for Beta Distribution

Now that we have established the method for determining the probability of detection, we use the beta distribution as the fluctuation model, $w(x)$:

$$w(x) = \frac{1}{\beta(a,b)}x^{a-1}(1-x)^{b-1}, \tag{26}$$

where $\beta(a,b) = \frac{\Gamma(a)\Gamma(b)}{\Gamma(a+b)}$.

The RCS measurements are rescaled to align the experimental mean to the corresponding mean of the beta distribution. Normalizing the variable y,

$$w(y) = w(\frac{x}{M}) = \frac{1}{\beta(a,b)}(\frac{x}{M})^{a-1}(1-\frac{x}{M})^{b-1}, \tag{27}$$

where $y = (x/M)$, $M = (m_1/\mu_\beta)$, and $\mu_\beta = [a/(a+b)]$.

The characteristic equation for the beta distribution is found by,

$$\left[\overline{C_N}(p)\right]_\beta = \int_{-\infty}^{\infty} w_\beta(x)C_1(p)dx \tag{28}$$

$$\left[\overline{C_N}(p)\right]_\beta = \int_{0}^{\infty} \frac{1}{\beta(a,b)}\frac{1}{M}w(\frac{x}{M})C_1(p)dx \tag{29}$$

33

$$:= \frac{1}{\beta(a,b)} \int_0^M \frac{x^{a-1}(M-x)^{b-1}}{M^{a+b-1}} \left\{ \frac{\exp\left[-(Nxp)/(p+1)\right]}{(p+1)^N} \right\} dx \ . \tag{30}$$

With the change of variable $x = Mt = \left(\frac{a+b}{a}\overline{x}t\right)$ ,

$$\left[\overline{C_N}(p)\right]_\beta = \frac{1}{\beta(a,b)} \int_0^1 t^{a-1} \frac{(1-t)^{b-1}\exp\{-Nt\overline{x}[\frac{a+b}{a}]p/(p+1)]\}}{(p+1)^N} dt \tag{31}$$

$$= \frac{1}{\beta(a,b)} \int_0^1 t^{a-1}(1-t)^{b-1}\frac{\exp\left(\frac{-NMtp}{p+1}\right)}{(p+1)^N} dt \ . \tag{32}$$

This result is directly related to the confluent hypergeometric function $_1F_1$,

$$_1F_1(a,c,z) = \frac{\Gamma(c)}{\Gamma(a)\Gamma(c-a)} \int_0^1 e^{zt}t^{a-1}(1-t)^{c-a-1}dt \tag{33}$$

as follows:

$$\left[\overline{C_N}(p)\right]_\beta = \frac{_1F_1\left[a, a+b, -\frac{NMp}{p+1}\right]}{(p+1)^N} \ . \tag{34}$$

This result is for the slow fluctuation case. The fast fluctuation case is related to the slow case as shown,

$$\overline{C_N}(p)_{fast} = \left[\overline{C_1}(p)_{slow}\right]^N \tag{35}$$

$$= \left[\frac{_1F_1(a, a+b, \frac{-MNp}{p+1})}{p+1}\right]^N \ . \tag{36}$$

Using these characteristic equations, a simple expression for $P_D$ can be obtained.

$$P_D = 1 - \int_0^{y_s} \mathcal{L}^{-1}\left[\overline{C_N}(p)\right] \ . \tag{37}$$

Kulp[22] has shown that the expression for $P_D$ can further be simplified as follows:

$$P_D = 1 - \int_{\epsilon-i\infty}^{\epsilon+i\infty} \frac{\overline{C_N}(p)\,\varepsilon\,\mathrm{xp}^{Y_s p}}{p} dp$$

$$= 1 - \mathcal{L}^{-1}\left(\frac{\overline{C_N}(p)}{p}\right)\bigg|_{y=Y_t} \ . \tag{38}$$

[22] Kulp, R.L. (1984) Detection Probabilities for Beta Distributed Scatter Cross Sections, *Electromagnetics*, 4(2-3):165-183

34

Kulp[23] has developed a computer code for the computation of detection probability versus signal-to-noise ratio curves. This code has been incorporated into a single program which determines all the necessary statistics of RCS, finds an appropriate beta distribution, and calculates the probability of detection for various sectors of aspect angle.

## 4.4 Analysis

For this analysis, we will use the computer generated RCS distributions of the cylinder. We use the entire range of aspect angles, $0 - 360°$, determine the moments about the mean and compute the beta parameters. The CDF plots are used to ensure the fit of the beta distribution to the data and the detection probabilities are computed for the various cases. The entire range of aspect angles is used in this analysis under the assumption of no knowledge of cylinder orientation. This analysis is thus kept to a theoretical level, that is, no real target scenarios are taken into account.

In the previous sections we have shown the PDFs and the CDFs for these cases. The probability of detection curves have been calculated for these cases and are presented in Figures 40 through 47. Figures 40 through 43 are the horizontal polarization (HH) cases and Figure 44 through Figure 47 are the vertical polarization (VV) cases. These detection probabilities have been determined for 10 and 50 noncoherently integrated pulses, and both the fast and slow fluctuating cases.

From the figures, the increase in the probability of detection with increasing bistatic angle is clear. However, the slow fluctuation cases show an extremely low probability of detection for large signal-to-noise ratios. This results from the shape and location of the cylinder PDFs for the $0 - 360°$ case. In this case, the PDFs are similar to the noise PDF, thereby creating a low probability of detection. Referring to Figure 18, it can be seen that if the signal-plus-noise PDF were similar to the noise PDF, the probability of detection would be low. The fast fluctuation cases make up for this low detection probability through the convolution of the characteristic equation with itself N-1 times.

## 5 CONCLUSIONS

This analysis has determined an appropriate characterizing function for bistatic RCS distributions, used this distribution in the computation of detection probabilities, and compared these probabilities for both the monostatic and several bistatic cases. A computer scattering code was used to calculate the monostatic and bistatic RCS of a cylinder as a function of aspect angle. The beta distribution provides the most accurate statistical description for the RCS distributions of the cylinder. This was shown through the CDF's and the implementation of the Kolmogorov-Smirnov two-sided test. This statistical model was used in the computation of detection probabilities for the cylinder. These detection probabilities were compared, and it was shown that the bistatic cases provide an increase in the probability of detection for the cylinder. This increase occurs at the large bistatic angles due to the reduced RCS amplitude fluctuation rate and the increase in the RCS.

[23]Kulp, R.L. (1983) *Detection Probabilities for Beta Distributed Signals*, JHU/APL Memorandum F1D(1)83-U-017.

The detection probabilities determined in this analysis are low for the given signal-to-noise ratios, due to the shape and location of the cylinder PDF's for the $0 - 360°$ case. The $0 - 360°$ sector was used in this analysis under the assumption of no knowledge of cylinder orientation relative to the radar. The knowledge of target trajectory and the allowance for changes in target orientation, relative to the radar, defines a sector of aspect angles. A sector comprises the various orientations, relative to the radar, that the target may have as it proceeds along its trajectory. An analysis of an actual radar system would take into consideration this zone of interest, computing the detection probabilities for these sectors of interest. This type of analysis may be considered for future work. An example of a zone analysis is included in Appendix C.

Another step is to perform this analysis on other objects and complex bodies. This analysis can also be completed using monostatic and bistatic RCS measurements rather than computer generated RCS. The bistatic and monostatic measurements of RCS for a given object could be completed, and by using the beta distribution, the detection probabilities can be determined. Various scenarios can be determined for the zones of interest for various targets. The final step would be the actual deployment of a bistatic radar system from which it could be determined whether or not it will provide greater performance than a monostatic system.

Figure 40. $P_D$ for HH Polarization: Fast Fluctuation Case, N=10, and 360° Sector Width



Figure 41. $P_D$ for HH Polarization: Slow Fluctuation Case, N=10, and 360° Sector Width
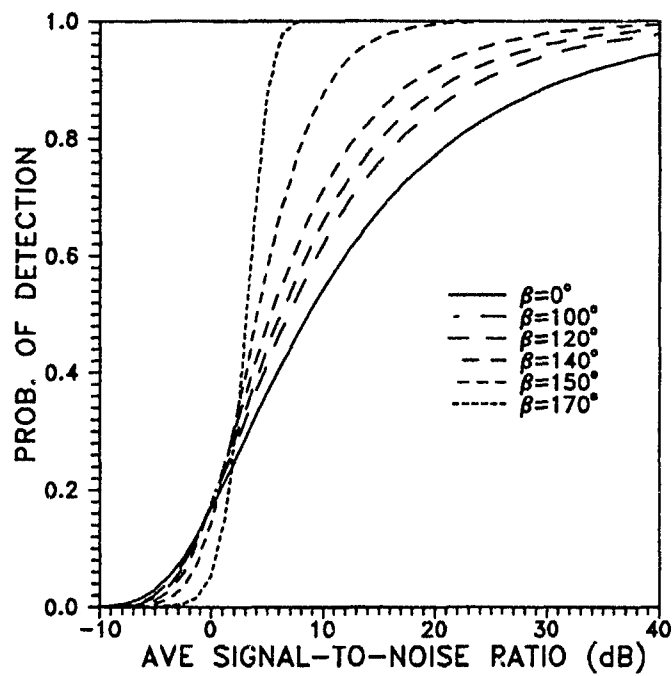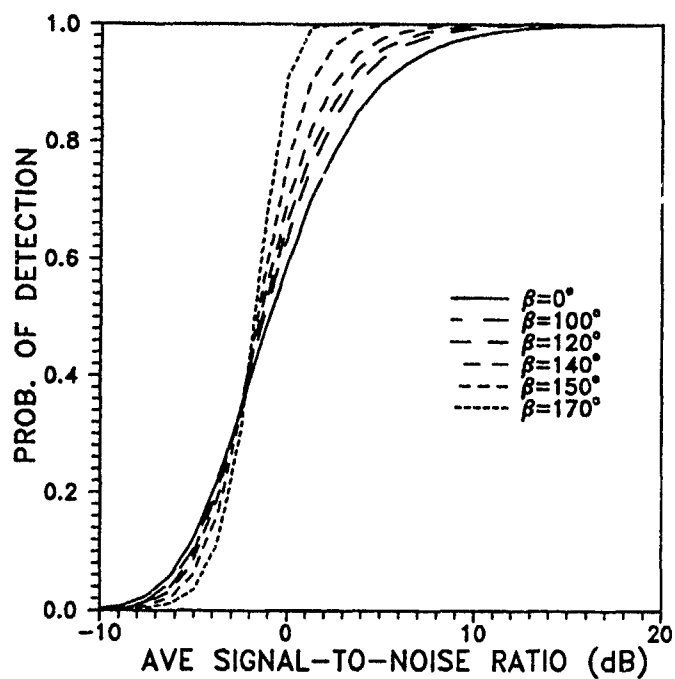
Figure 42. $P_D$ for HH Polarization: Fast Fluctuation Case, N=50, and 360° Sector Width



Figure 43. $P_D$ for HH Polarization: Slow Fluctuation Case, N=50, and 360° Sector Width

Figure 44. $P_D$ for VV Polarization: Fast Fluctuation Case, N=10, and 360° Sector Width
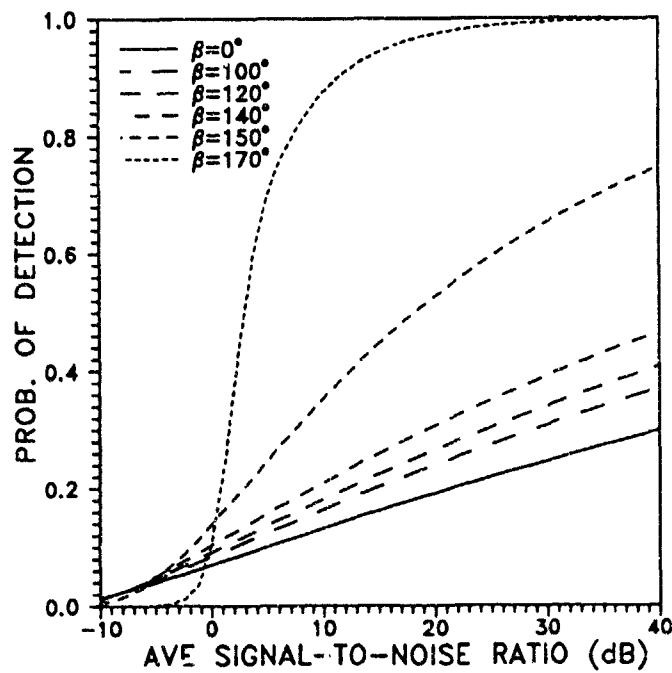


Figure 45. $P_D$ for VV Polarization: Slow Fluctuation Case, N=10, and 360° Sector Width

Figure 46. $P_D$ for VV Polarization: Fast Fluctuation Case, N=50, and 360° Sector Width



Figure 47. $P_D$ for VV Polarization: Slow Fluctuation Case, N=50, and 360° Sector Width
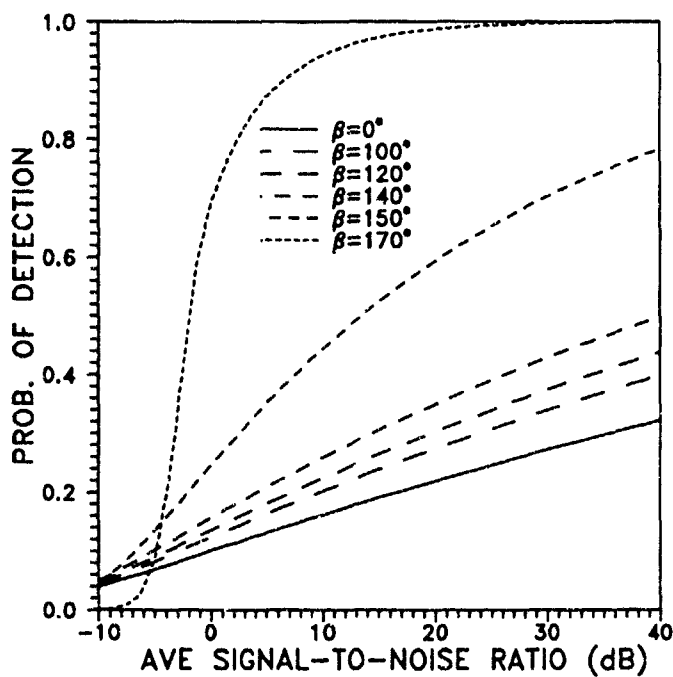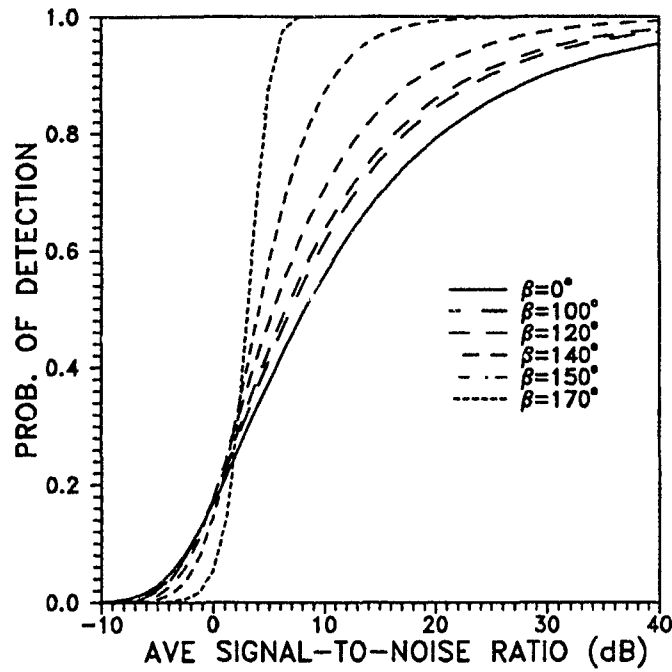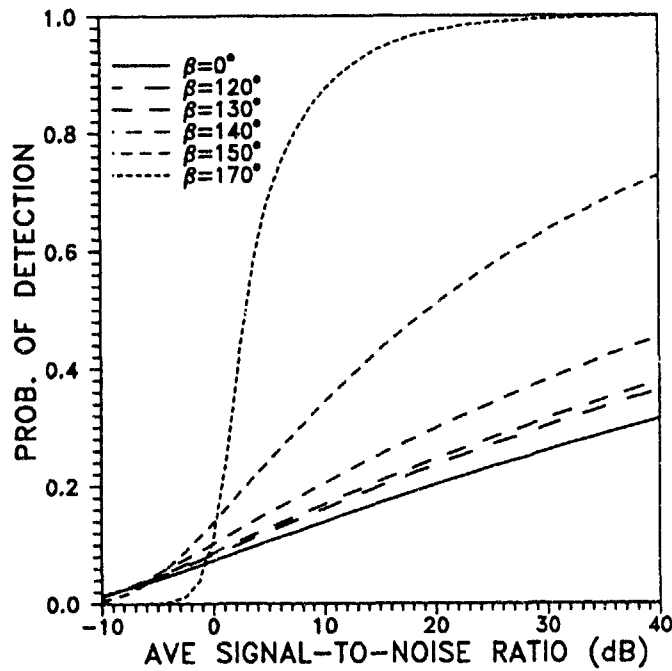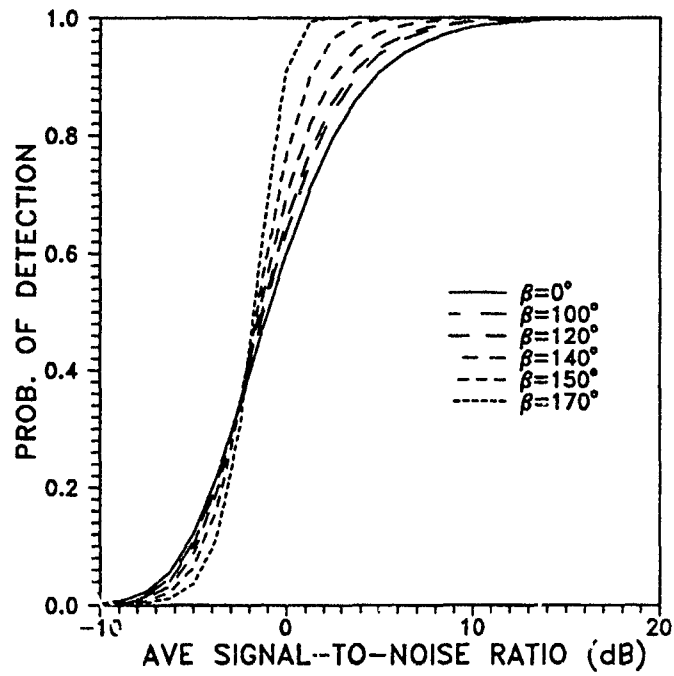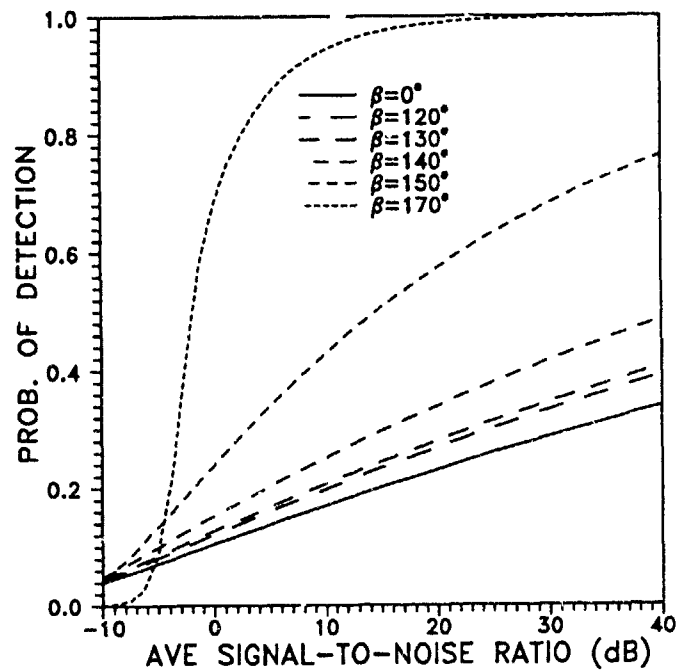
# References

1. Skolnik, M.I. (1970) *Radar Handbook,* McGraw-Hill Inc., New York.

2. Skolnik, M.I. (1961) An Analysis of Bistatic Radar, *IRE Trans. Aero. and Nav. Electron.,* 8:19-27.

3. Mitchell, B. (1988) European Firms Target Development of Bistatic Radar, *Microwaves & RF,* 27(3):49-54.

4. Paddison, F.C.,Follin, J.W., and Mitchell, F. (1985) Large Bistatic Angle Radar Cross Section of a Right Circular Cylinder, *Electromagnetics,* 5:63-77.

5. Follin, J.W., Paddison, F.C., and Maffett, A.L. (1984) Statistics of Radar Cross Section Scintillations, *Journal of Electromagnetics,* 4:139-164.

6. Marcum, J.I. (1960) A Statistical Theory of Target Detection by a Pulsed Radar, *IRE Trans. Inform. Theory,* IT-6:145-267.

7. Swerling, P. (1960) Probability of Detection for Fluctuating Targets, *IRE Trans. Inform. Theory,* IT-6:65-217.

8. Barton, D.K. (1988) *Modern Radar System Analysis,* Artech House, Norwood, MA.

9. Mie, G. (1908) *Ann. d. Physik,* 25:377-442.

10. DiBeneditto, J.P. (1984) *Bistatic Scattering From Conducting Calibration Spheres,* RADC-TR-84-93, Hanscom AFB, MA.

11. Cha, C., Michels, J., and Starczewski, E. (1989) An RCS Analysis of Generic Airborne Vehicles Dependence Upon Frequency and Bistatic Angle, *Proceedings of the 1989 IEEE National Radar Conference* pp 214-219.

12. Fisz, M. (1963) *Probability Theory and Mathematical Statistics, Radar Systems and Components,* D. Van Nostrand Co., New York.

13. Daniel, W.W. (1978) *Applied Nonparametric Statistics,* Houghton Mifflin Co., Boston, MA.

14. Campbell, G.A. and Foster, R.M. (1947) *Fourier Integrals for Practical Applications,* Van Nostrand Reinhold, Princeton, New Jersey.

15. Kulp, R.L. (1984) Detection Probabilities for Beta Distributed Scatter Cross Sections, *Journal of Electromagnetics,* 4(2-3):165-183.

16. Kulp, R.L. (1983) *Detection Probabilities for Beta Distributed Signals*, JHU/APL Memorandum F1D(1)83-U-017.

# Appendix A
## Cylinder Statistics

This appendix contains tables of the statistics from the cylinder RCS. The cases presented are for monostatic and bistatic angles of 100 to 170°. The cases presented are for the entire aspect angle from 0 to 360°. Both the horizontal and vertical polarization cases are presented in this appendix. This should give the reader a feel for the values that we determined from the cylinder RCS. The reader should note that for the bistatic angle of 160°, the beta shape parameter $b$ is negative. As these parameters are defined to be positive, we are unable to determine a beta distribution for these cases.

Table 2. Cylinder RCS Statistics, Horizontal Polarization

| Bistatic Angle | Mean | Width | Skewness | Kurtosis | a | b |
|---|---|---|---|---|---|---|
| 0° | 0.0157 | 28.3284 | 50.1243 | 93.8176 | 0.0307 | 6.9485 |
| 100° | 0.0232 | 19.9555 | 33.6959 | 59.1234 | 0.0410 | 4.7024 |
| 110° | 0.0256 | 18.1498 | 30.4369 | 52.6852 | 0.0447 | 4.4881 |
| 120° | 0.0286 | 16.6.47 | 27.2395 | 45.5192 | 0.0469 | 3.7388 |
| 130° | 0.0319 | 15.7109 | 24.2581 | 37.9245 | 0.0455 | 2.6199 |
| 140° | 0.0389 | 12.6739 | 19.6004 | 30.3474 | 0.0567 | 2.7016 |
| 150° | 0.0594 | 6.7397 | 12.4517 | 22.6078 | 0.1364 | 12.9265 |
| 160° | 0.1309 | 1.7103 | 4.8187 | 13.5669 | 0.8006 | -6.6776 |
| 170° | 0.2703 | 0.2766 | -0.2401 | -0.8614 | 0.7552 | 0.4633 |

Table 3. Cylinder RCS Statistics, Vertical Polarization

| Bistatic Angle | Mean | Width | Skewness | Kurtosis | a | b |
|---|---|---|---|---|---|---|
| 0° | 0.0162 | 26.8847 | 48.2677 | 92.1035 | 0.0329 | 8.1036 |
| 100° | 0.0229 | 20.3024 | 34.0374 | 59.3335 | 0.0399 | 4.4473 |
| 110° | 0.0249 | 19.1721 | 31.2964 | 52.7978 | 0.0406 | 3.6837 |
| 120° | 0.0276 | 17.8051 | 28.2334 | 45.9152 | 0.0419 | 3.0566 |
| 130° | 0.0311 | 16.2742 | 24.8317 | 38.4728 | 0.0431 | 2.4340 |
| 140° | 0.0388 | 12.9114 | 19.6725 | 30.0566 | 0.0542 | 2.4696 |
| 150° | 0.0600 | 6.8705 | 12.1934 | 21.3486 | 0.1277 | 8.0436 |
| 160° | 0.1244 | 2.0196 | 4.8769 | 12.0899 | 0.5911 | -9.8005 |
| 170° | 0.4722 | 0.3052 | -0.216 | -1.001 | 0.6981 | 0.4597 |

# Appendix B

## K-S Statistics

This appendix contains tables of the Kolmogorov-Smirnov two-sided test for the cylinder RCS. The cases given are for monostatic and bistatic angles from 100 to 170°. The cases presented are for the entire aspect angle from 0 to 360°. Both the horizontal and vertical polarization cases are presented in this appendix. This should be sufficient for the reader to obtain a feel for the values that were obtained by the application of the Kolmogorov-Smirnov two-sided test and the approximate number of cases that met the desired criteria. Once again the reader should note that for the bistatic angle of 160°, the beta parameter $b$ is negative and we are unable to determine a beta distribution. This is reflected in the tables included in this appendix.

Table 4. K-S Statistics For Cylinder, Horizontal Polarization

| Bistatic Angle | $D_\beta$ | $D_{X_2}$ | $D_{X_4}$ | $D_{LN}$ |
|---|---|---|---|---|
| 0° | 0.2475 | 0.6238 | 0.7327 | 0.3861 |
| 100° | 0.2277 | 0.6039 | 0.7129 | 0.2673 |
| 110° | 0.2178 | 0.5941 | 0.7029 | 0.2971 |
| 120° | 0.2178 | 0.6039 | 0.7129 | 0.3465 |
| 130° | 0.2079 | 0.6436 | 0.7426 | 0.3168 |
| 140° | 0.2079 | 0.5842 | 0.6931 | 0.3267 |
| 150° | 0.2277 | 0.8713 | 0.6931 | 0.6139 |
| 160° | — | — | — | — |
| 170° | 0.1980 | 0.3267 | 0.2772 | 0.4059 |

Table 5. K-S Statistics For Cylinder, Vertical Polarization

| Bistatic Angle | $D_\beta$ | $D_{X_2}$ | $D_{X_4}$ | $D_{LN}$ |
|---|---|---|---|---|
| 0° | 0.2475 | 0.5644 | 0.6931 | 0.4059 |
| 100° | 0.2178 | 0.6238 | 0.7327 | 0.3564 |
| 110° | 0.2178 | 0.6436 | 0.7426 | 0.3267 |
| 120° | 0.2178 | 0.6535 | 0.7525 | 0.2772 |
| 130° | 0.2079 | 0.6634 | 0.7426 | 0.2574 |
| 140° | 0.1980 | 0.6039 | 0.7129 | 0.2971 |
| 150° | 0.2178 | 5644 | 0.4455 | 0.5248 |
| 160° | — | — | — | — |
| 170° | 0.1980 | 0.3168 | 0.2673 | 0.3861 |

# Appendix C

## Zone Analysis

In this appendix, a sector of the cylinder RCS is used in the computation and comparison of detection probabilities for both the monostatic and bistatic cases. An analysis of target detectability would follow in a similar fashion. A zone of interest is determined through the interpretation of the target's path relative to the radar system. Given the path of the target, a sector of aspect angles can be determined that will correspond to changes in orientation as the target proceeds along its path. This sector of aspect angles is the zone and the RCS for the target within this sector is used in the computation of detection probabilities.

The $345 - 15°$ sector of aspect angles for the cylinder RCS is used in this analysis. Thus the zone is a $30°$ sector about the end of the cylinder. A beta distribution is fit to the data, and the detection probabilities are found and compared for both the monostatic and bistatic cases. These detection probabilities are shown in Figure 48 for the slow fluctuation case and Figure 49 for the fast fluctuation case. From these figures it is shown that the bistatic case provides an increase in the detection probabilities. These detection probabilities are more reasonable for the given signal-to-noise ratios than was found using the $0 - 360°$ sectors.

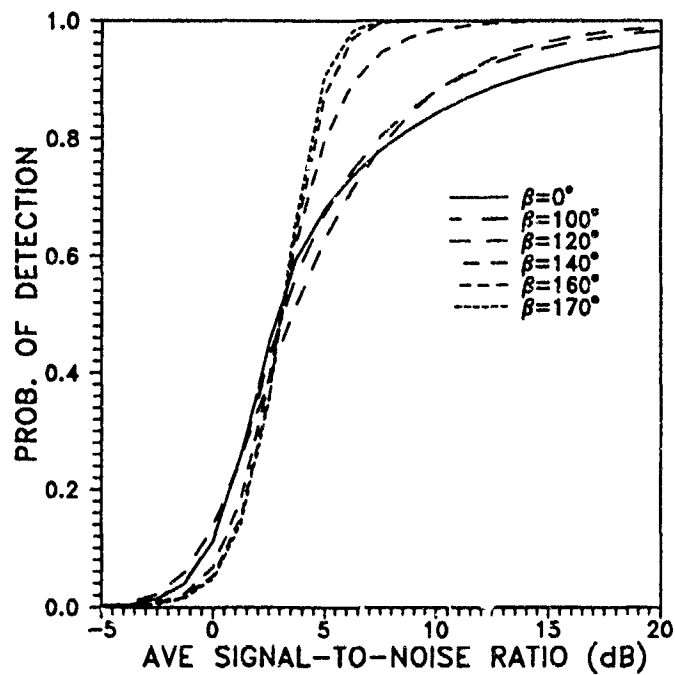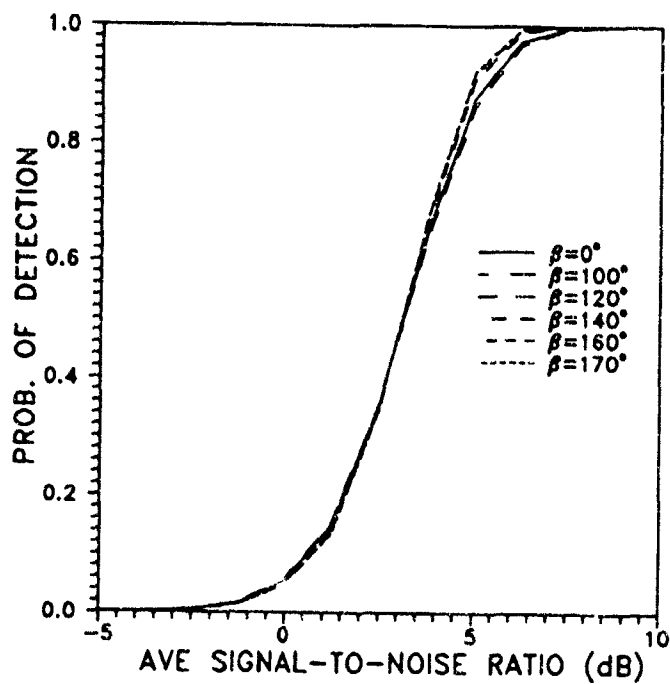Figure 48. $P_D$ for HH Polarization: Slow Fluctuation Case, N=10, and 30° Sector Width



Figure 49. $P_D$ for HH Polarization: Fast Fluctuation Case. N=10, and 30° Sector Width

48